Global Nonhydrostatic Modeling Using Voronoi Meshes

Bill Skamarock, Joe Klemp, Michael Duda, Laura Fowler, Sang-Hun Park
National Center for Atmospheric Research

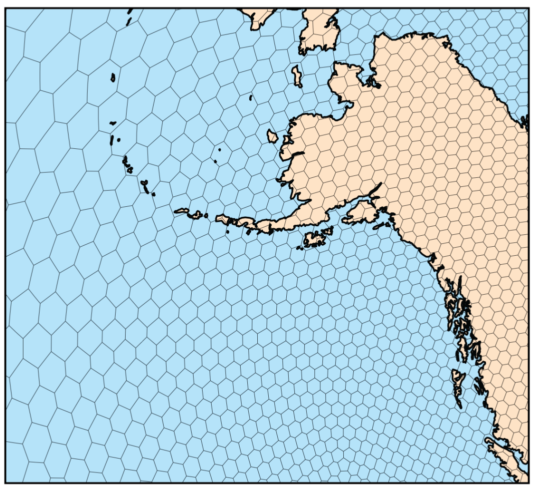

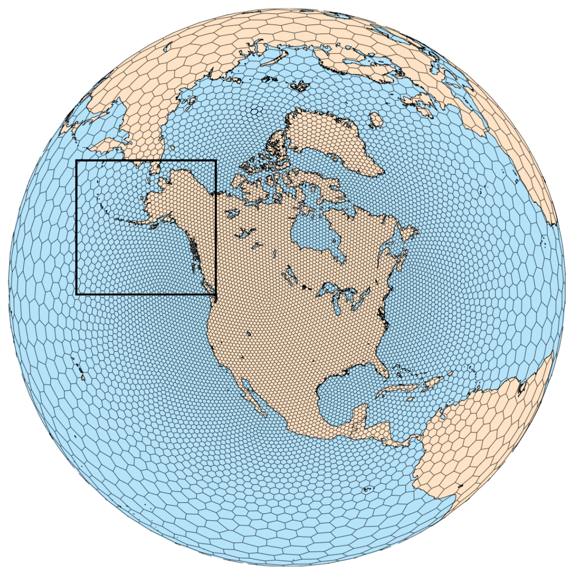

Topics

Motivation

Voronoi mesh

Nonhydrostatic equations

Discretization

Uniform-mesh results

Variable-resolution mesh results

MPAS
Model for Prediction Across Scales

Los Alamos NATIONAL LABORATORY EST. 1943

U.S. DEPARTMENT OF ENERGY | Office of Science

NSF

NESL

Motivation
Mesh flexibility:
North
American
refinement

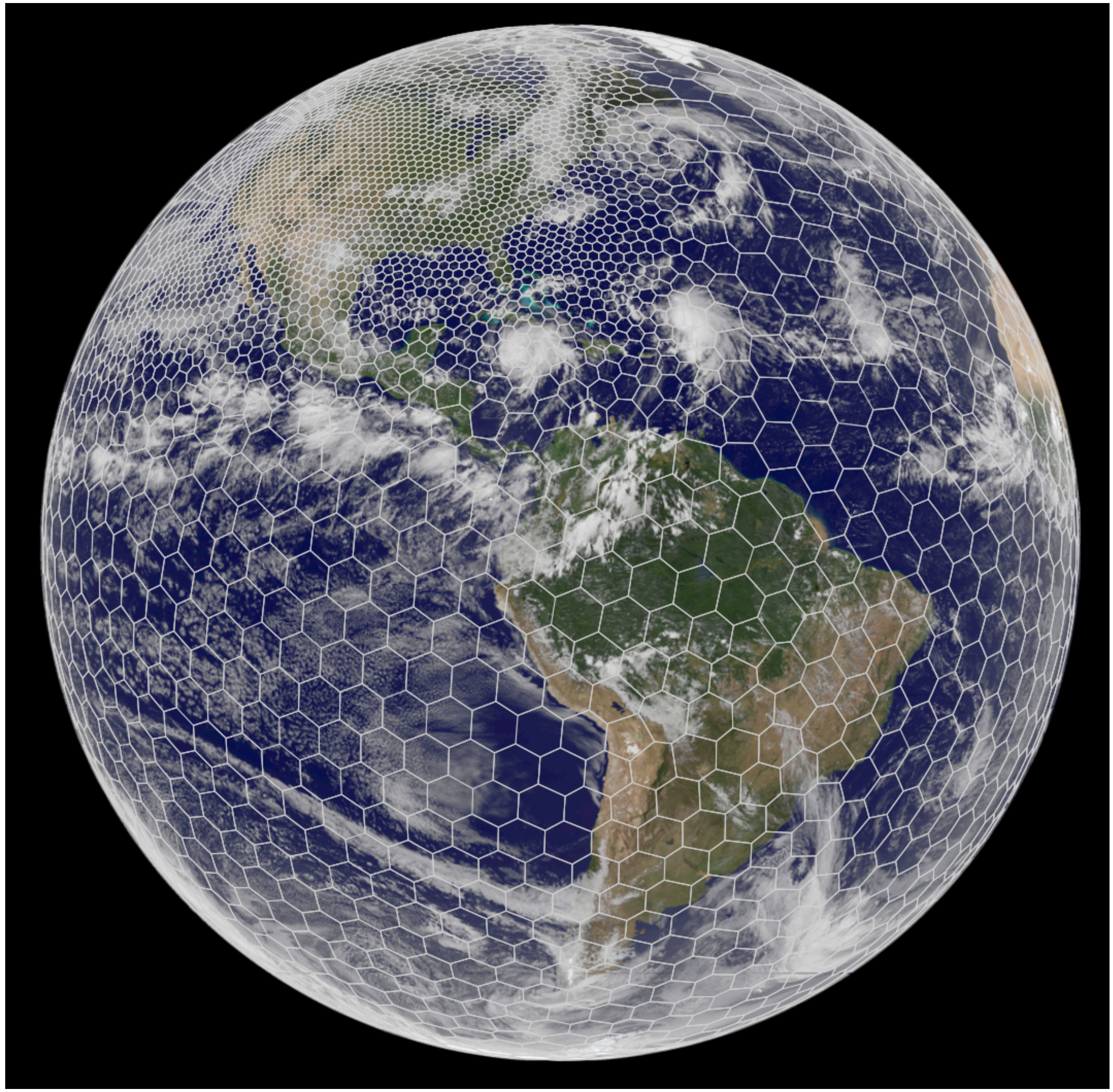

Motivation

Mesh flexibility:
Refinement
for equatorial
convection

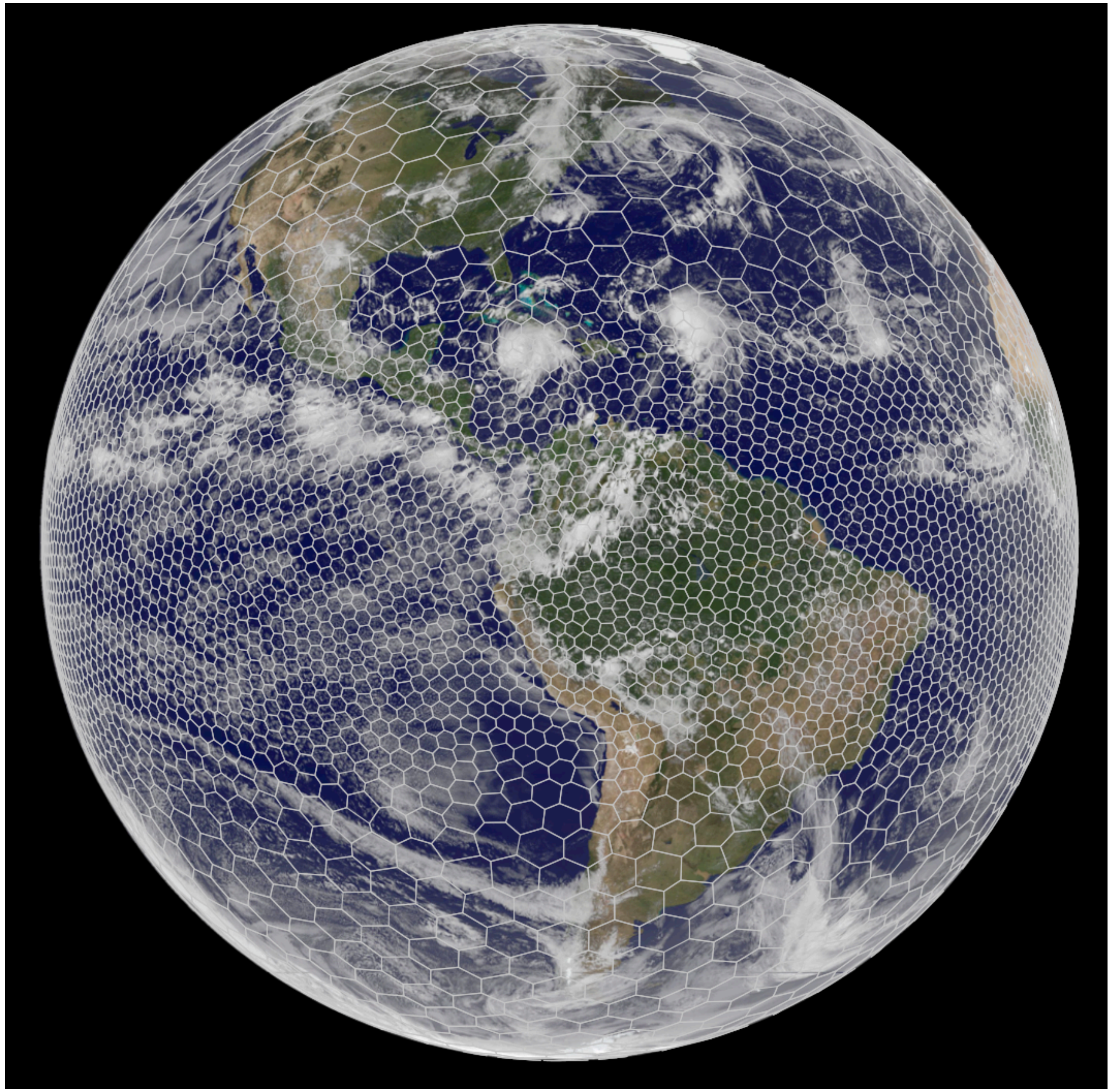

Motivation

Mesh flexibility:
Refinement around the Andes

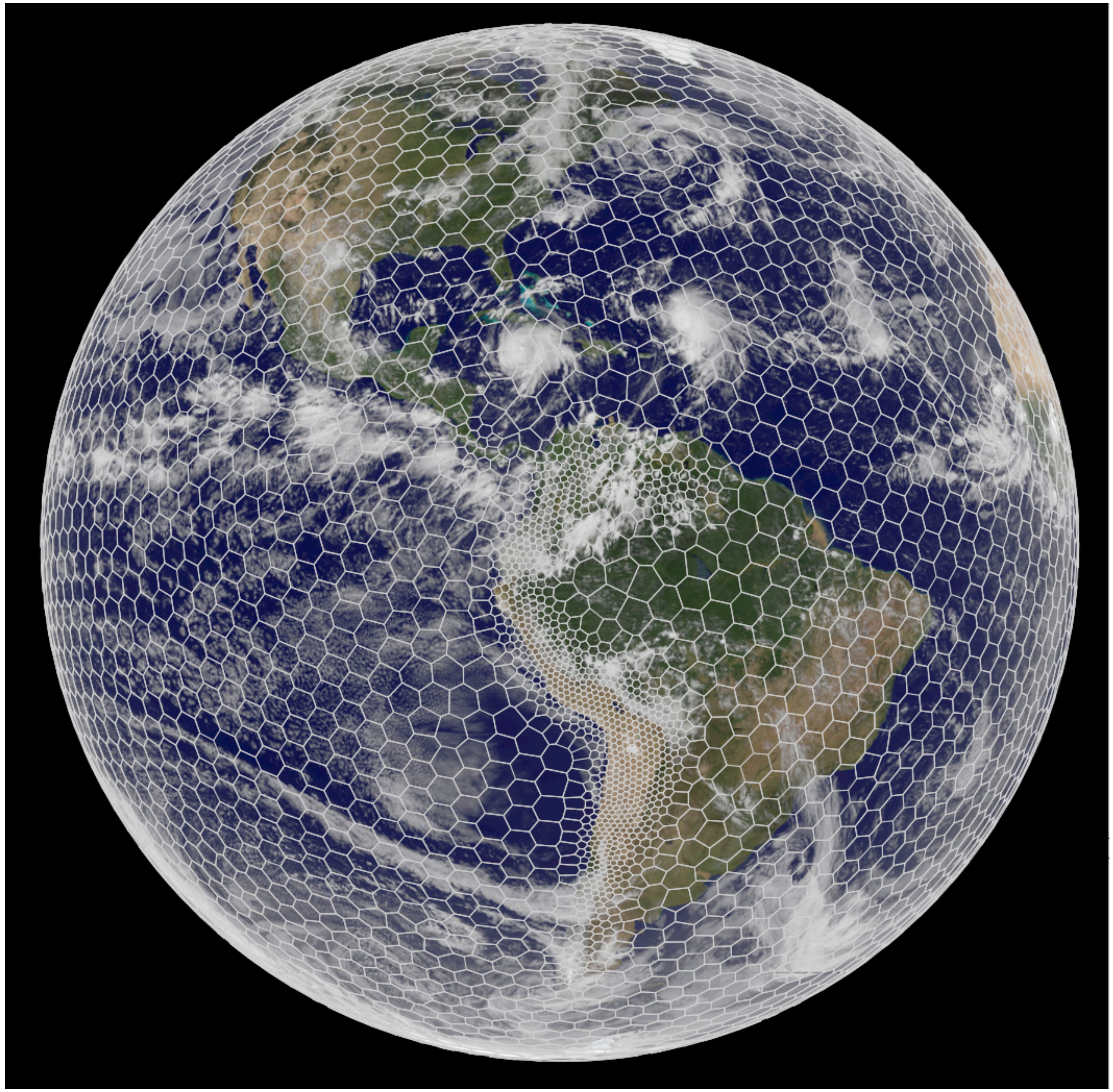

Motivation: Global Mesh and Integration Options

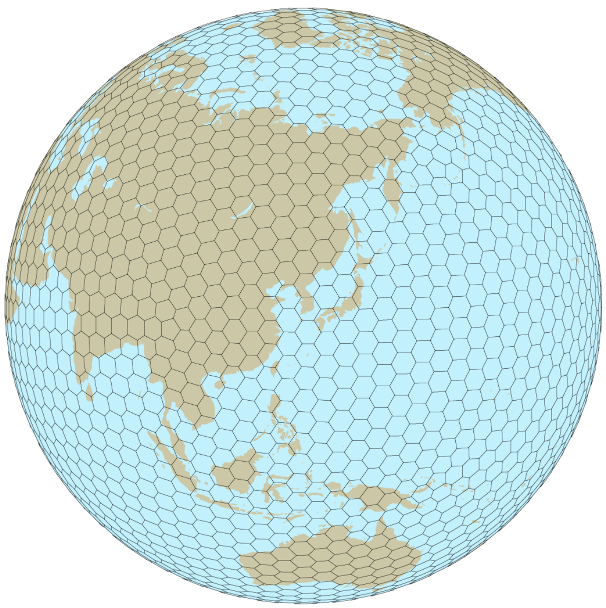

Global Uniform Mesh

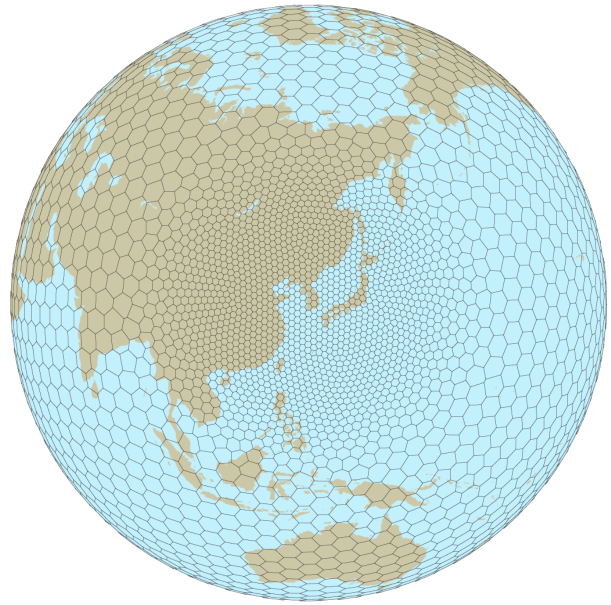

Global Variable Resolution Mesh

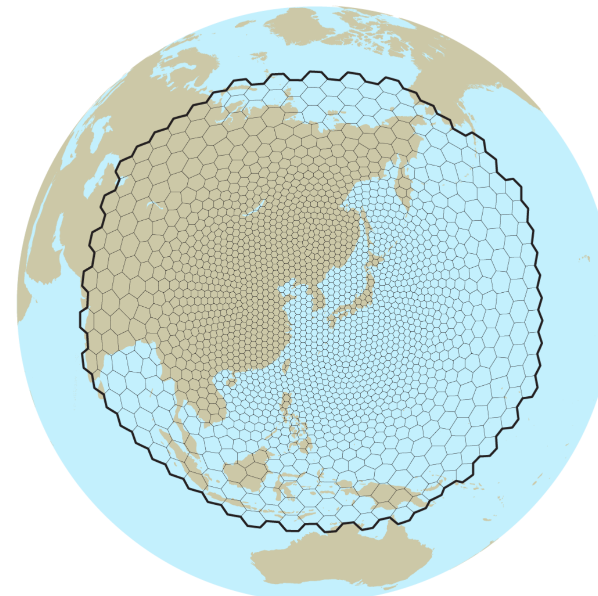

Regional Mesh - driven by

(1) previous global MPAS run
(no spatial interpolation needed!)
(2) other global model run
(3) analyses

Voronoi meshes allows us to cleanly incorporate both downscaling and upscaling effects (avoiding the problems in traditional grid nesting) and to assess the accuracy of the traditional downscaling approaches used in regional climate and NWP applications.

Centroidal Voronoi Meshes

<u>Unstructured spherical centroidal Voronoi meshes</u>

Mostly *hexagons*, some pentagons and 7-sided cells.
Cell centers are at cell center-of-mass.
Lines connecting cell centers intersect cell edges at right angles.
Lines connecting cell centers are bisected by cell edge.
Mesh generation uses a density function.
Uniform resolution – traditional icosahedral mesh.

<u>C-grid</u>

Solve for normal velocities on cell edges.

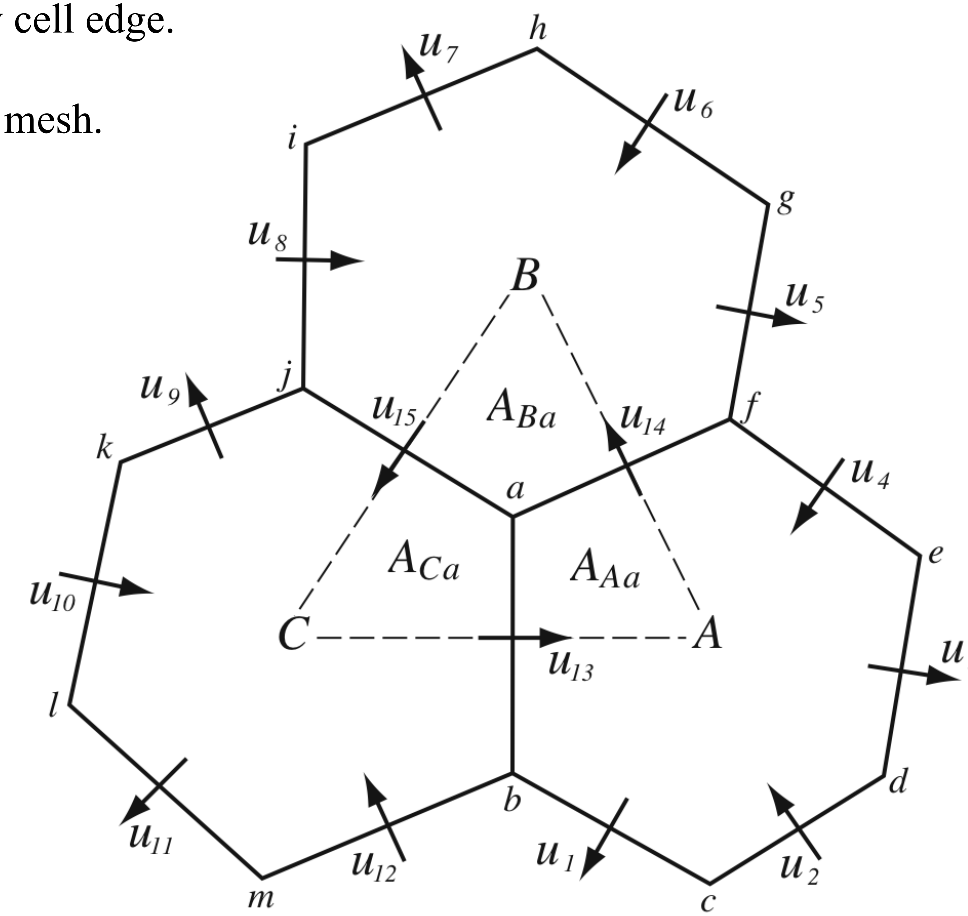

Centroidal Voronoi Meshes: Lloyd's Method

Given an initial set of generating points, Lloyd's method may be used to arrive at a CVT:

1. Begin with any set of initial points (the generating point set)
2. Construct a Voronoi diagram for the set
3. Locate the mass centroid of each Voronoi cell
4. Move each generating point to the mass centroid of its Voronoi cell
5. Repeat 2-4 to convergence

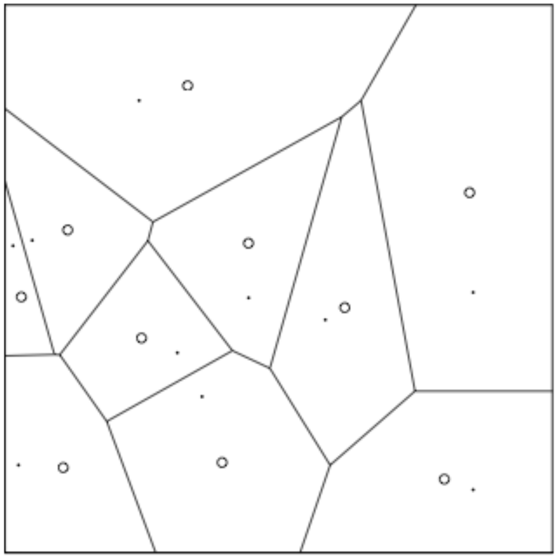

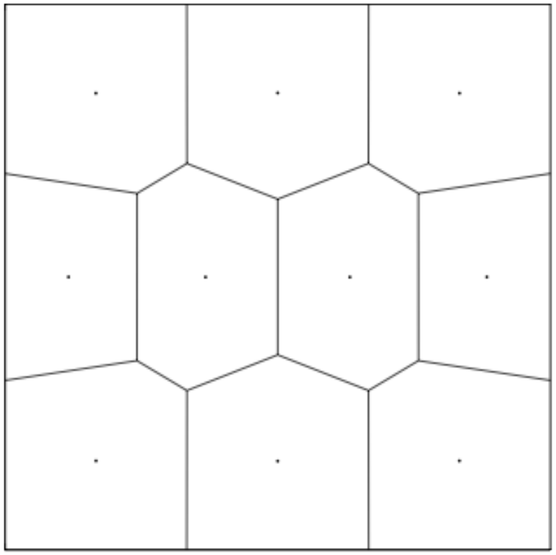

From Du et al. (1999)

MacQueen's method, a randomized alternative to Lloyd's method, may also be used; no Voronoi diagrams need to be constructed, but convergence is generally much slower.

Centroidal Voronoi Meshes: Voronoi diagram

Fortune's Method
for constructing the Voronoi diagram

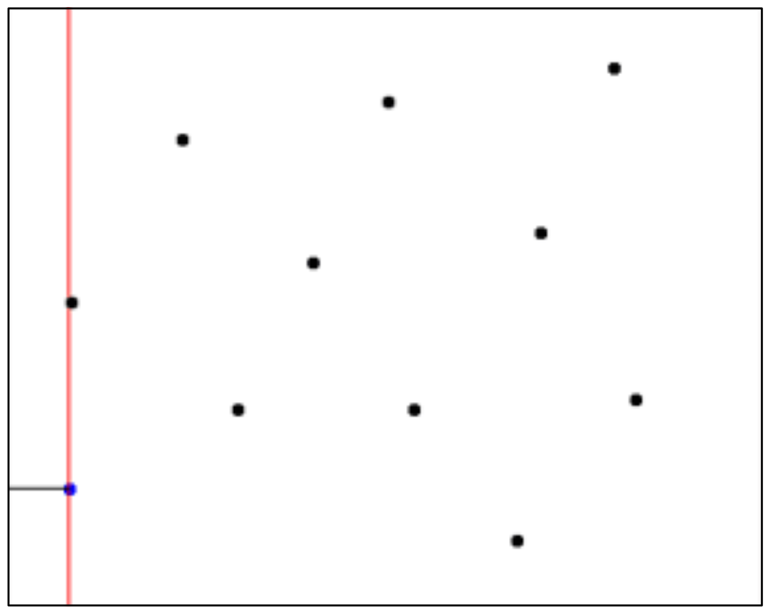

http://en.wikipedia.org/wiki/Fortune's_algorithm

Centroidal Voronoi Meshes: Mesh Generation

Mesh generation
beginning from an
icosahedral mesh.
All points are *free*.

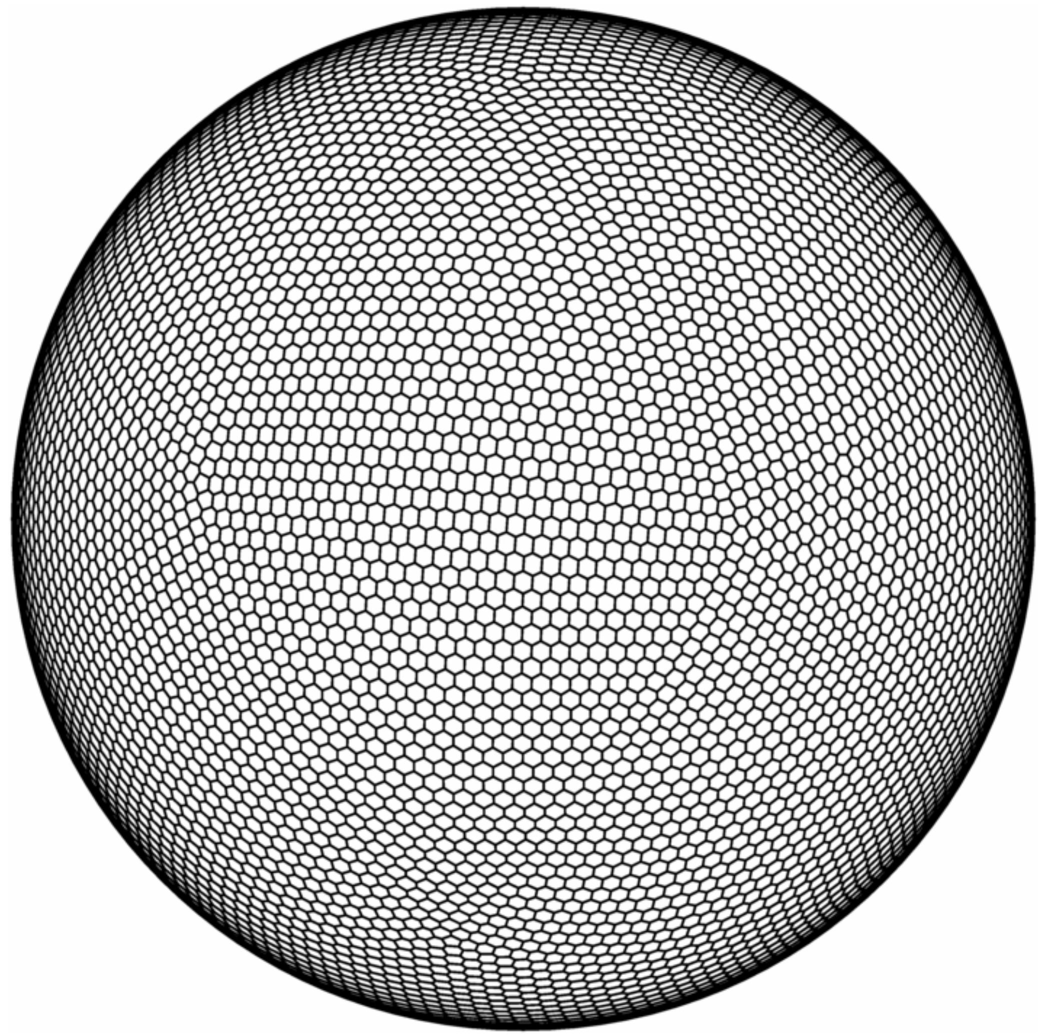

Centroidal Voronoi Meshes: Mesh Generation

Mesh generation beginning from an icosahedral mesh with constrained refinement. Only points in the refinement region are *free*.

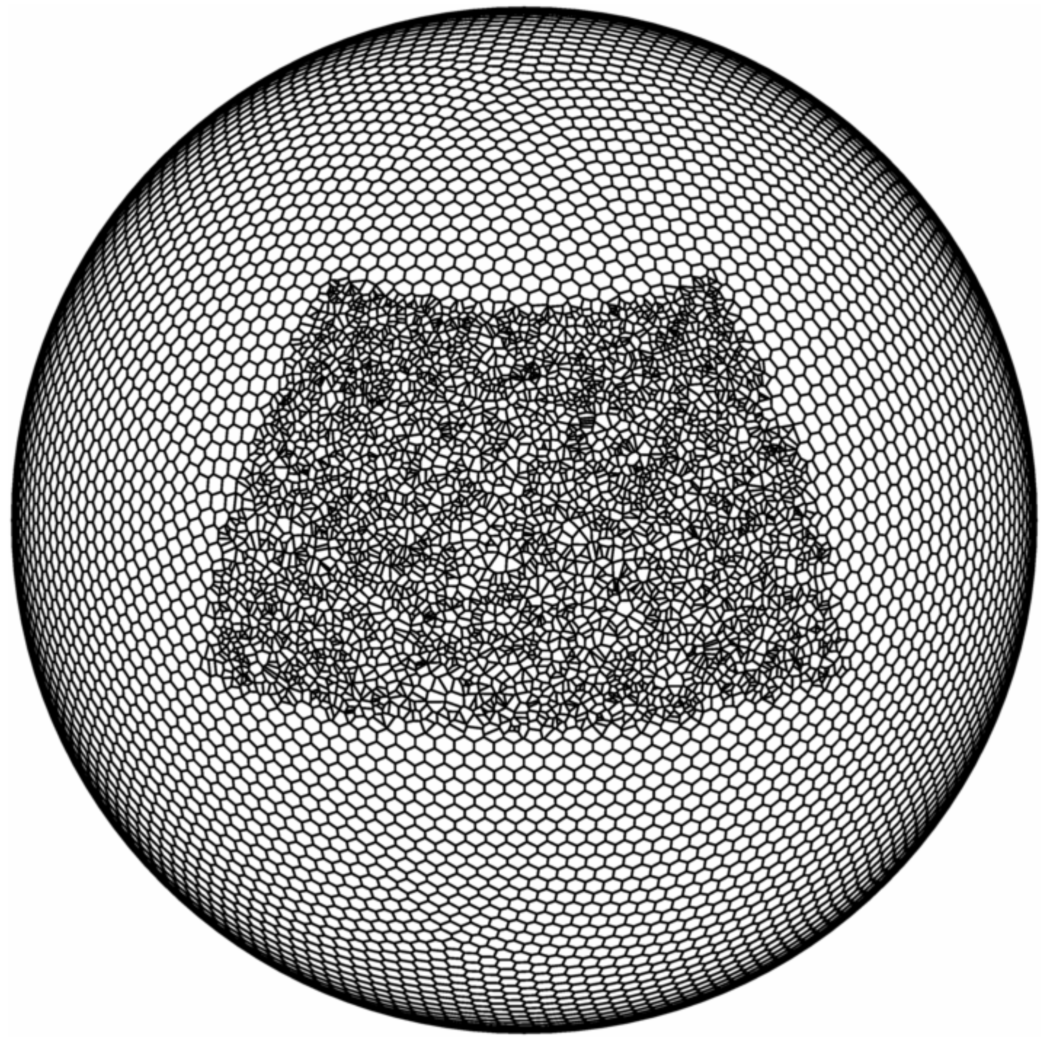

MPAS Nonhydrostatic Atmospheric Solver

Nonhydrostatic formulation

Equations

- Prognostic equations for coupled variables.
- Generalized height coordinate.
- Horizontally vector invariant eqn set.
- Continuity equation for dry air mass.
- Thermodynamic equation for coupled potential temperature.

Time integration scheme

As in Advanced Research WRF -
Split-explicit Runge-Kutta (3rd order)

Variables:

$(U,V,\Omega,\Theta,Q_j) = \tilde{\rho}_d \cdot (u,v,\dot{\eta},\theta,q_j)$

Vertical coordinate:

$z = \zeta + A(\zeta)\, h_s(x,y,\zeta)$

Prognostic equations:

$$\frac{\partial \mathbf{V}_H}{\partial t} = -\frac{\rho_d}{\rho_m}\left[\nabla_\zeta\left(\frac{p}{\zeta_z}\right) - \frac{\partial \mathbf{z}_H p}{\partial \zeta}\right] - \eta\, \mathbf{k} \times \mathbf{V}_H$$
$$- \mathbf{v}_H \nabla_\zeta \cdot \mathbf{V} - \frac{\partial \Omega \mathbf{v}_H}{\partial \zeta} - \rho_d \nabla_\zeta K - eW\cos\alpha_r - \frac{uW}{r_e} + \mathbf{F}_{V_H},$$

$$\frac{\partial W}{\partial t} = -\frac{\rho_d}{\rho_m}\left[\frac{\partial p}{\partial \zeta} + g\tilde{\rho}_m\right] - (\nabla \cdot \mathbf{v} W)_\zeta$$
$$+ \frac{uU + vV}{r_e} + e\,(U\cos\alpha_r - V\sin\alpha_r) + F_W,$$

$$\frac{\partial \Theta_m}{\partial t} = -(\nabla \cdot \mathbf{V}\, \theta_m)_\zeta + F_{\Theta_m},$$

$$\frac{\partial \tilde{\rho}_d}{\partial t} = -(\nabla \cdot \mathbf{V})_\zeta,$$

$$\frac{\partial Q_j}{\partial t} = -(\nabla \cdot \mathbf{V}\, q_j)_\zeta + \rho_d S_j + F_{Q_j},$$

Diagnostics and definitions:

$$\theta_m = \theta[1 + (R_v/R_d) q_v] \qquad p = p_0 \left(\frac{R_d \zeta_z \Theta_m}{p_0}\right)^\gamma$$

$$\frac{\rho_m}{\rho_d} = 1 + q_v + q_c + q_r + \ldots$$

MPAS Nonhydrostatic Atmospheric Solver

Prognostic equations:

$$\frac{\partial \boldsymbol{V}_H}{\partial t} = -\frac{\rho_d}{\rho_m}\left[\nabla_\zeta\left(\frac{p}{\zeta_z}\right) - \frac{\partial \boldsymbol{z}_H p}{\partial \zeta}\right] - \eta\, \boldsymbol{k} \times \boldsymbol{V}_H$$
$$- \boldsymbol{v}_H \nabla_\zeta \cdot \boldsymbol{V} - \frac{\partial \Omega \boldsymbol{v}_H}{\partial \zeta} - \rho_d \nabla_\zeta K - eW\cos\alpha_r - \frac{uW}{r_e} + \boldsymbol{F}_{V_H},$$

$$\frac{\partial W}{\partial t} = -\frac{\rho_d}{\rho_m}\left[\frac{\partial p}{\partial \zeta} + g\tilde{\rho}_m\right] - (\nabla \cdot \boldsymbol{v} W)_\zeta$$
$$+ \frac{uU + vV}{r_e} + e(U\cos\alpha_r - V\sin\alpha_r) + F_W,$$

$$\frac{\partial \Theta_m}{\partial t} = -(\nabla \cdot \boldsymbol{V}\, \theta_m)_\zeta + F_{\Theta_m},$$

$$\frac{\partial \tilde{\rho}_d}{\partial t} = -(\nabla \cdot \boldsymbol{V})_\zeta,$$

$$\frac{\partial Q_j}{\partial t} = -(\nabla \cdot \boldsymbol{V}\, q_j)_\zeta + \rho_d S_j + F_{Q_j},$$

(1) Gradient operators

(2) Flux divergence operators

(3) Nonlinear Coriolis term

Operators on the Voronoi Mesh - Pressure and KE gradients

$$\frac{\partial \mathbf{V}_H}{\partial t} = -\frac{\rho_d}{\rho_m}\left[\nabla_\zeta\left(\frac{p}{\zeta_z}\right) - \frac{\partial \mathbf{z}_H p}{\partial \zeta}\right] - \eta\, \boldsymbol{k} \times \mathbf{V}_H$$
$$- \boldsymbol{v}_H \nabla_\zeta \cdot \boldsymbol{V} - \frac{\partial \Omega \boldsymbol{v}_H}{\partial \zeta} - \rho_d \nabla_\zeta K - eW \cos\alpha_r - \frac{uW}{r_e} + \boldsymbol{F}_{V_H},$$

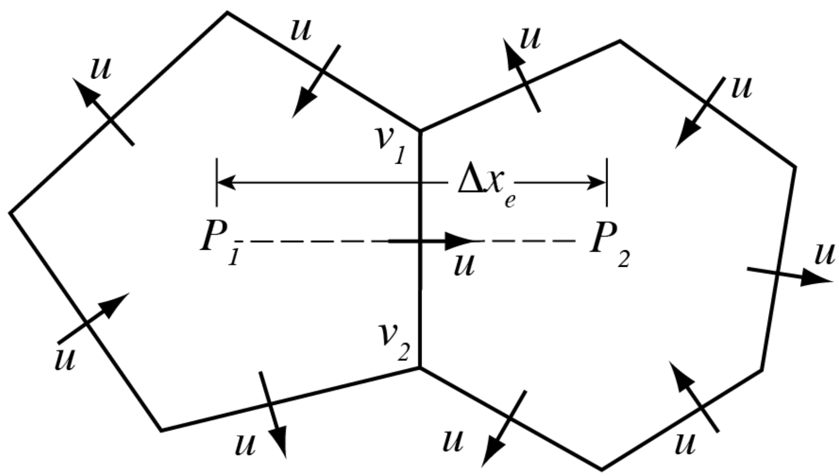

On the Voronoi mesh, P_1P_2 is perpendicular to v_1v_2 and is bisected by v_1v_2, hence $P_x \sim (P_2\text{-}P_1)\Delta x_e^{-1}$ is 2nd order accurate.

Operators on the Voronoi Mesh – Flux Divergence

Transport equation, conservative form: $$\frac{\partial(\rho\psi)}{\partial t} = -\nabla \cdot \mathbf{V}(\rho\psi)$$

Finite-Volume formulation, Integrate over cell: $$\int_D \left[\frac{\partial}{\partial t}(\rho\psi) = -\nabla \cdot \mathbf{V}(\rho\psi) \right] dV$$

Apply divergence theorum: $$\frac{\partial(\overline{\rho\psi})}{\partial t} = -\frac{1}{V} \int_{\Sigma} (\rho\psi)\, \mathbf{V} \cdot \mathbf{n}\; d\sigma$$

Discretize in time and space: $$(\rho\psi)_i^{t+\Delta t} = (\rho\psi)_i^t - \Delta t \, \frac{1}{A_i} \sum_{n_{e_i}} d_{e_i} \overline{(\rho \mathbf{V} \cdot \mathbf{n}_{e_i})\psi}$$

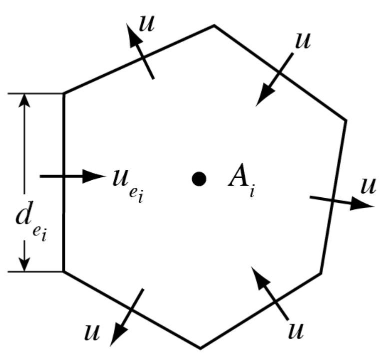

Velocity divergence operator is 2nd-order accurate for edge-centered velocities.

Operators on the Voronoi Mesh – Flux Divergence

Computing the flux - consider 1D transport (e.g. from WRF)

$$\frac{\partial(u\psi_i)}{\partial x} = \frac{1}{\Delta x}\left[F_{i+1/2}(u\psi) - F_{i-1/2}(u\psi)\right] + O(\Delta x^p).$$

2nd-order flux:

$$F(u,\psi)_{i+1/2} = u_{i+1/2}\left[\frac{1}{2}\left(\psi_{i+1} + \psi_i\right)\right]$$

3rd and 4th-order fluxes:

$$F(u,\psi)_{i+1/2} = u_{i+1/2}\left[\frac{1}{2}\left(\psi_{i+1} + \psi_i\right) - \frac{1}{12}\left(\delta_x^2\psi_{i+1} + \delta_x^2\psi_i\right) + sign(u)\,\frac{\beta}{12}\left(\delta_x^2\psi_{i+1} - \delta_x^2\psi_i\right)\right]$$

where $\delta_x^2\psi_i = \psi_{i-1} - 2\psi_i + \psi_{i+1}$

Operators on the Voronoi Mesh – Flux Divergence

Recognizing $$\delta_x^2 \psi = \Delta x^2 \frac{\partial^2 \psi}{\partial x^2} + O(\Delta x^4)$$

We recast the 3rd and 4th order flux for the hexagonal grid as

$$F(u,\psi)_{i+1/2} = u_{i+1/2} \left[\frac{1}{2} (\psi_{i+1} + \psi_i) - \Delta x_e^2 \frac{1}{12} \left\{ \left(\frac{\partial^2 \psi}{\partial x^2} \right)_{i+1} + \left(\frac{\partial^2 \psi}{\partial x^2} \right)_i \right\} + sign(u)\, \Delta x_e^2 \frac{\beta}{12} \left\{ \left(\frac{\partial^2 \psi}{\partial x^2} \right)_{i+1} - \left(\frac{\partial^2 \psi}{\partial x^2} \right)_i \right\} \right]$$

where x is the direction normal to the cell edge and i and $i+1$ are cell centers.
We use the least-squares-fit polynomial to compute the second derivatives.

Operators on the Voronoi Mesh – Flux Divergence

$$F(u,\psi)_{i+1/2} = u_{i+1/2}\left[\frac{1}{2}\left(\psi_{i+1}+\psi_i\right) - \Delta x_e^2 \frac{1}{12}\left\{\left(\frac{\partial^2\psi}{\partial x^2}\right)_{i+1} + \left(\frac{\partial^2\psi}{\partial x^2}\right)_i\right\} + sign(u)\,\Delta x_e^2 \frac{\beta}{12}\left\{\left(\frac{\partial^2\psi}{\partial x^2}\right)_{i+1} - \left(\frac{\partial^2\psi}{\partial x^2}\right)_i\right\}\right]$$

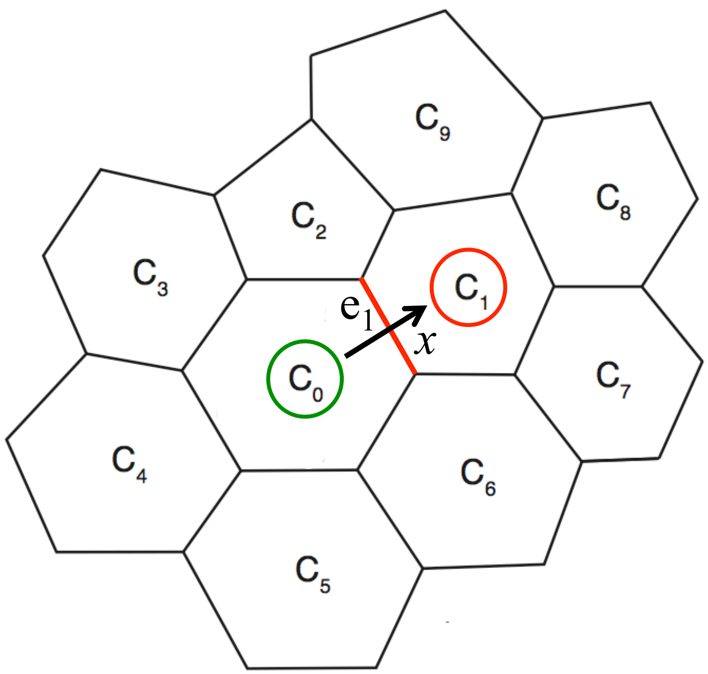

Edge e_1 has weights for computing second derivatives normal to e_1 at cell centers C_0 and C_1.

The weights for C_0 apply to cell centers C_0 through C_6, and the weights for C_1 apply to cell centers C_0 - C_2 and C_6 - C_9.

Operators on the Voronoi Mesh – 'nonlinear Coriolis force'

$$\frac{\partial \boldsymbol{V}_H}{\partial t} = -\frac{\rho_d}{\rho_m}\left[\boldsymbol{\nabla}_\zeta\left(\frac{p}{\zeta_z}\right) - \frac{\partial z_H p}{\partial \zeta}\right] - \eta\,\boldsymbol{k} \times \boldsymbol{V}_H$$
$$- \boldsymbol{v}_H \boldsymbol{\nabla}_\zeta \cdot \boldsymbol{V} - \frac{\partial \Omega \boldsymbol{v}_H}{\partial \zeta} - \rho_d \boldsymbol{\nabla}_\zeta K - eW\cos\alpha_r - \frac{uW}{r_e} + \boldsymbol{F}_{V_H},$$

Vorticity is computed by evaluating the circulation around the triangles. Vorticity *lives* on the vertices.

First, the linear piece: $f\ \boldsymbol{k}\ x\ \boldsymbol{V}_H$

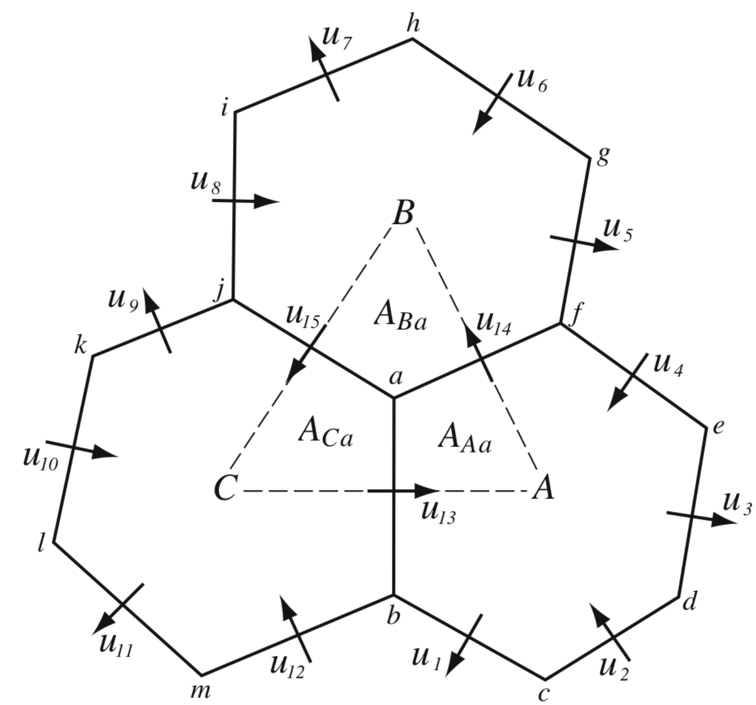

Operators on the Voronoi Mesh – 'nonlinear Coriolis force'

$$\frac{\partial \mathbf{V}_H}{\partial t} = -\frac{\rho_d}{\rho_m}\left[\nabla_\zeta\left(\frac{p}{\zeta_z}\right) - \frac{\partial \mathbf{z}_H p}{\partial \zeta}\right] - \eta\, \boldsymbol{k} \times \mathbf{V}_H$$
$$- \boldsymbol{v}_H \nabla_\zeta \cdot \boldsymbol{V} - \frac{\partial \Omega \boldsymbol{v}_H}{\partial \zeta} - \rho_d \nabla_\zeta K - eW\cos\alpha_r - \frac{uW}{r_e} + \boldsymbol{F}_{V_H},$$

Vorticity is computed by evaluating the circulation around the triangles.
Vorticity *lives* on the vertices.

First, the linear piece: $f\ \boldsymbol{k}\ x\ \boldsymbol{V_H}$

How do we compute the tangential velocity on the cell faces needed in the Coriolis term?

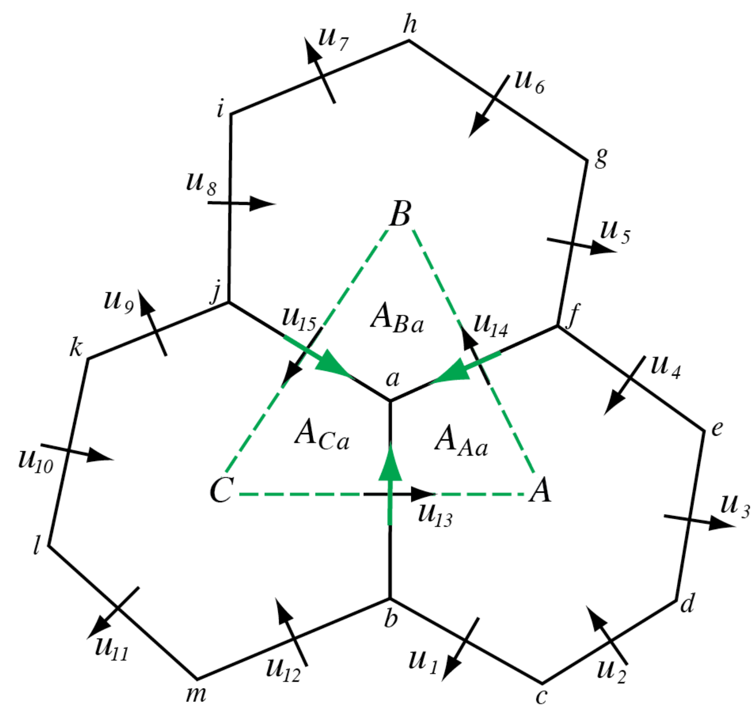

Operators on the Voronoi Mesh – ‘nonlinear Coriolis force’

$$\frac{\partial \boldsymbol{V}_H}{\partial t} = -\frac{\rho_d}{\rho_m}\left[\boldsymbol{\nabla}_\zeta\left(\frac{p}{\zeta_z}\right) - \frac{\partial \boldsymbol{z}_H p}{\partial \zeta}\right] - \eta\, \boldsymbol{k} \times \boldsymbol{V}_H$$
$$- \boldsymbol{v}_H \boldsymbol{\nabla}_\zeta \cdot \boldsymbol{V} - \frac{\partial \Omega \boldsymbol{v}_H}{\partial \zeta} - \rho_d \boldsymbol{\nabla}_\zeta K - eW\cos\alpha_r - \frac{uW}{r_e} + \boldsymbol{F}_{V_H},$$

Linear piece: $f\ \boldsymbol{k} \times \boldsymbol{V_H}$

Simplest approach: Construct tangential velocities from weighted sum of the four nearest neighbors.

Result: physically stationary geostrophic modes (geostrophically-balanced flow) will not be stationary in the discrete system; the solver is unusable.

(Nickovic et al, MWR 2002)

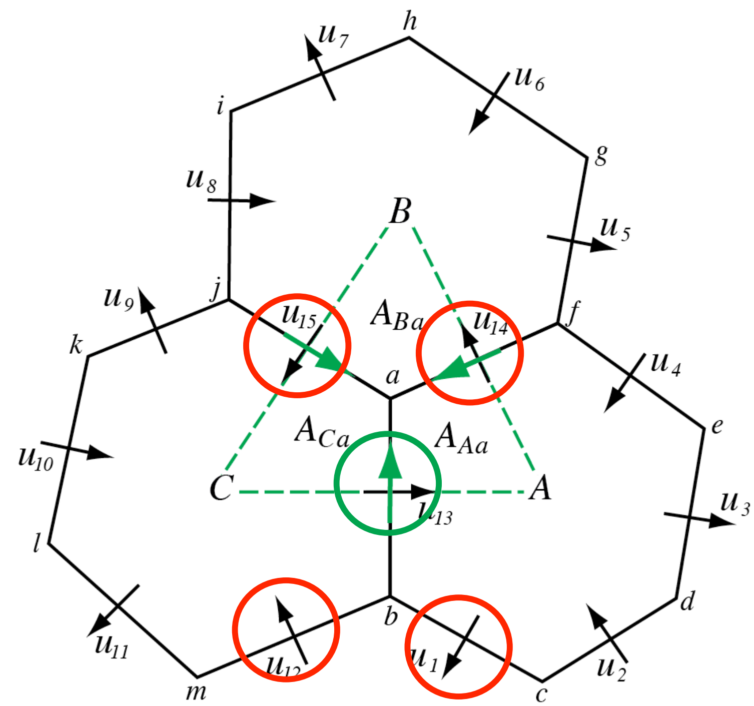

Operators on the Voronoi Mesh – ‘nonlinear Coriolis force’

Linear piece: $f\ \boldsymbol{k}\ x\ \boldsymbol{V_H}$

$$\partial_t u_1 + g\delta_{x_1} h + \frac{f}{\sqrt{3}}(u_{31} - u_{21}) = 0$$

$$\partial_t u_2 + g\delta_{x_2} h + \frac{f}{\sqrt{3}}(u_{12} - u_{32}) = 0$$

$$\partial_t u_3 + g\delta_{x_3} h + \frac{f}{\sqrt{3}}(u_{23} - u_{13}) = 0$$

$$\partial_t h + \tfrac{2}{3} H(\delta_{x_1} u_1 + \delta_{x_2} u_2 + \delta_{x_3} u_3) = 0$$

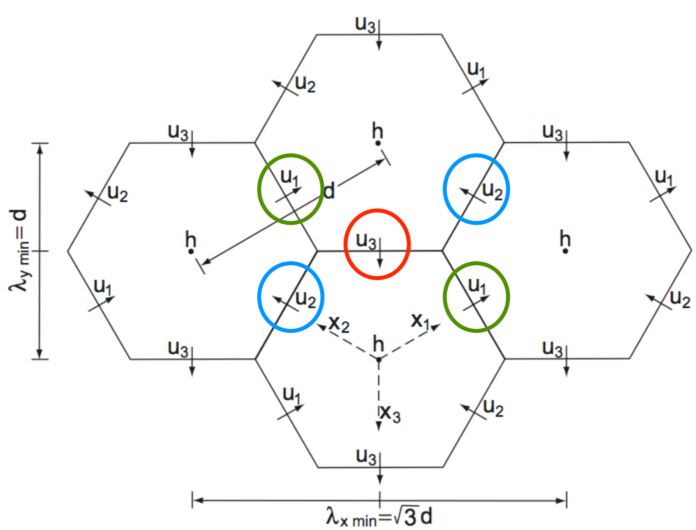

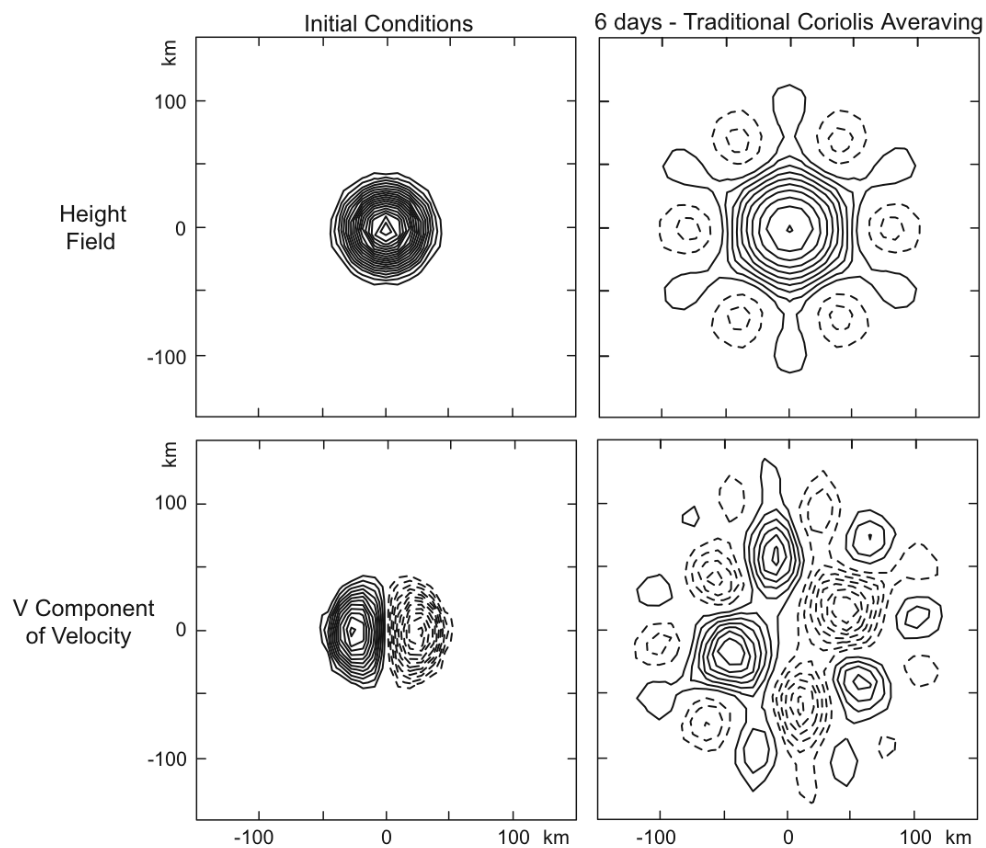

Operators on the Voronoi Mesh – ‘nonlinear Coriolis force’

Linear piece: $f\ \boldsymbol{k} \times \boldsymbol{V_H}$

(Thuburn et al, 2009 JCP)

$$\partial_t u_1 + g\delta_{x_1} h + \frac{f}{\sqrt{3}}(u_{31} - u_{21}) = 0$$

$$\partial_t u_2 + g\delta_{x_2} h + \frac{f}{\sqrt{3}}(u_{12} - u_{32}) = 0$$

$$\partial_t u_3 + g\delta_{x_3} h + \frac{f}{\sqrt{3}}(u_{23} - u_{13}) = 0$$

$$\partial_t h + \tfrac{2}{3} H(\delta_{x_1} u_1 + \delta_{x_2} u_2 + \delta_{x_3} u_3) = 0$$

$$u_{21} = \tfrac{1}{3}\overline{u_2}^{x_3} + \tfrac{2}{3}\overline{\overline{u_2}^{x_1}}^{x_2}, \quad u_{31} = \tfrac{1}{3}\overline{u_3}^{x_2} + \tfrac{2}{3}\overline{\overline{u_3}^{x_1}}^{x_3},$$

$$u_{12} = \tfrac{1}{3}\overline{u_1}^{x_3} + \tfrac{2}{3}\overline{\overline{u_1}^{x_1}}^{x_2}, \quad u_{32} = \tfrac{1}{3}\overline{u_3}^{x_1} + \tfrac{2}{3}\overline{\overline{u_3}^{x_2}}^{x_3},$$

$$u_{13} = \tfrac{1}{3}\overline{u_1}^{x_2} + \tfrac{2}{3}\overline{\overline{u_1}^{x_1}}^{x_3}, \quad u_{23} = \tfrac{1}{3}\overline{u_2}^{x_1} + \tfrac{2}{3}\overline{\overline{u_2}^{x_2}}^{x_3}$$

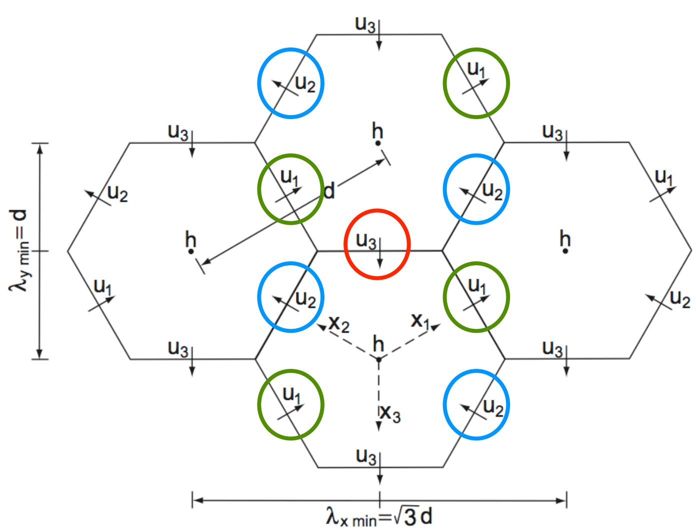

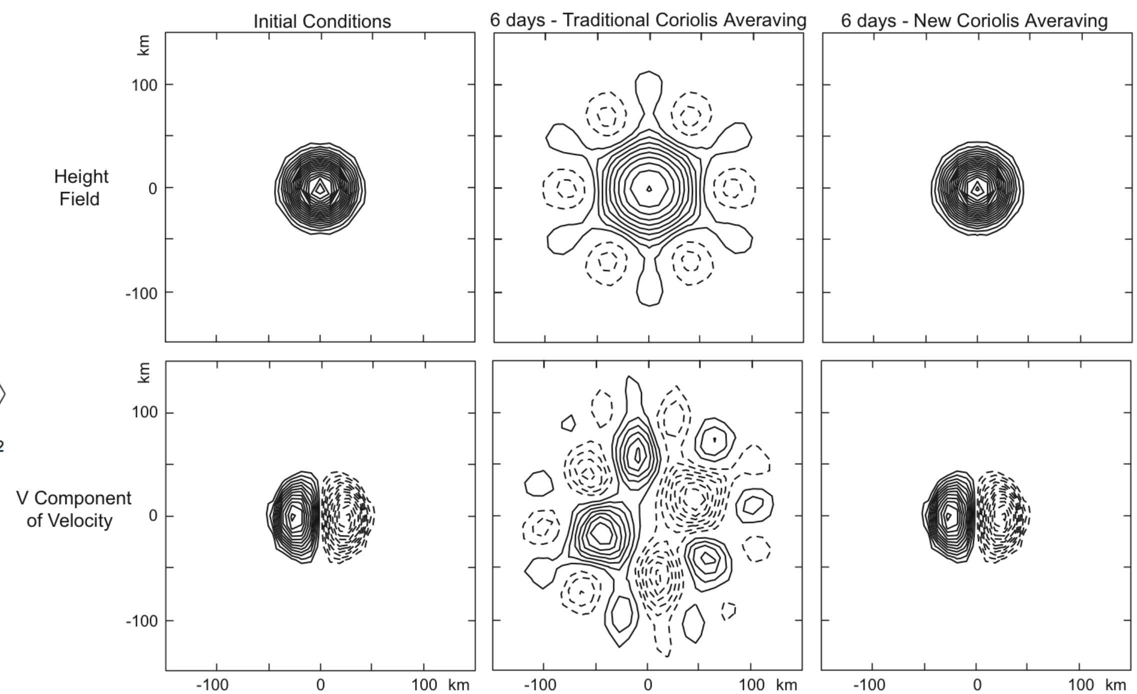

Operators on the Voronoi Mesh – 'nonlinear Coriolis force'

Why does this work?

In the discrete analogue of vorticity equation (ξ_τ=-fδ_a), the divergence δ_a on the Delaunay triangulation is identical to the divergence δ_A on the Voronoi hexagons used in the height equation (h_t=-Hδ_A) integrated over the triangle.

$$A_a\delta_a = \frac{A_A\delta_A + A_B\delta_B + A_C\delta_C}{6}$$

Divergence δ_A in hexagon A:

$$A_A\delta_A = \sum_{i=1}^{6} l_i u_i \cdot \mathbf{n}_i$$

Divergence δ_a in triangle ABC:

$$A_a\xi_t = -fA_a\delta_a = f\sum_{j=1}^{3} d_j u_j^{\perp} \cdot \mathbf{n}_j$$

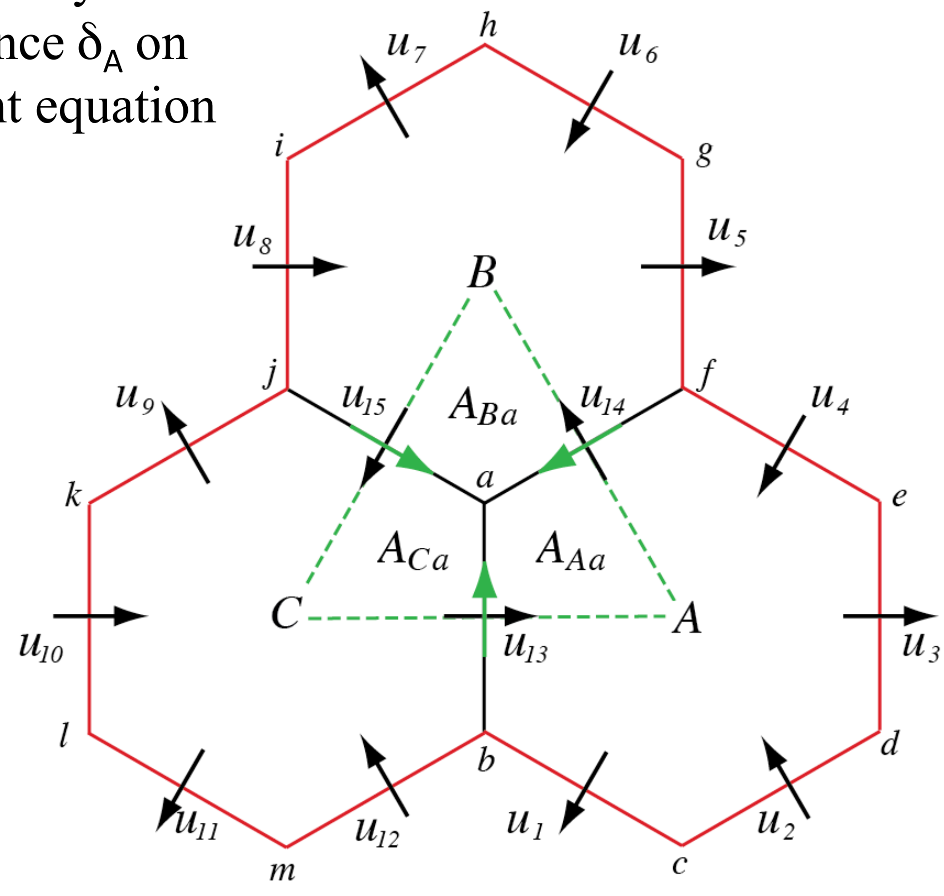

Operators on the Voronoi Mesh – 'nonlinear Coriolis force'

Linear piece: $f\ \boldsymbol{k} \times \boldsymbol{V_H}$

Generalization for the Voronoi mesh:

Construct tangential velocities from weighted sum of normal velocities on edges of adjacent hexagons.

$$d_e\, u_e^{\perp} = \sum_j w_e^j\, l_j\, u_j$$

Result: geostrophic modes are stationary; local and global mass and PV conservation is satisfied on the dual (triangular) mesh (for the SW equations).

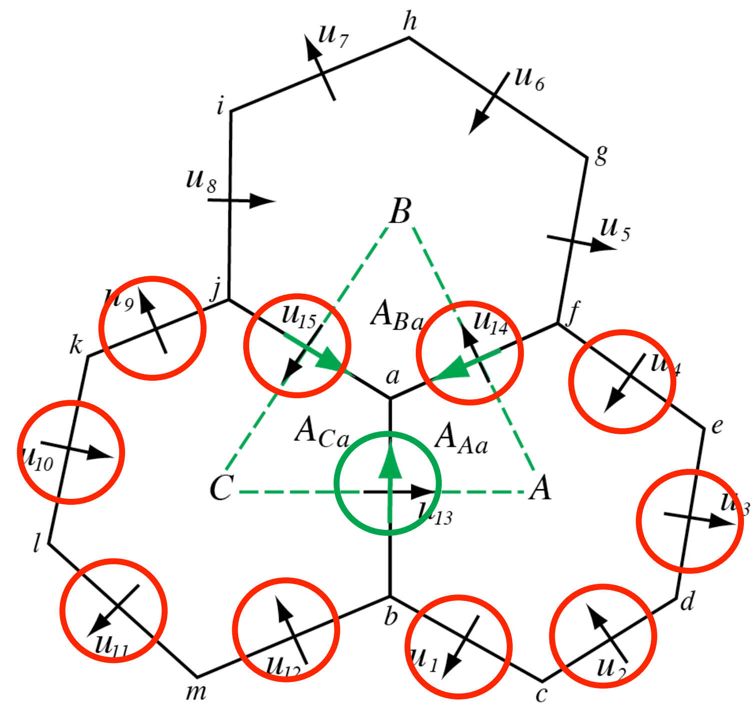

Operators on the Voronoi Mesh – ‘nonlinear Coriolis force’

$$\frac{\partial \boldsymbol{V}_H}{\partial t} = -\frac{\rho_d}{\rho_m}\left[\boldsymbol{\nabla}_\zeta\left(\frac{p}{\zeta_z}\right) - \frac{\partial z_H p}{\partial \zeta}\right] - \eta\,\boldsymbol{k}\times\boldsymbol{V}_H$$
$$-\boldsymbol{v}_H \boldsymbol{\nabla}_\zeta\cdot\boldsymbol{V} - \frac{\partial \Omega \boldsymbol{v}_H}{\partial \zeta} - \rho_d \boldsymbol{\nabla}_\zeta K - eW\cos\alpha_r - \frac{uW}{r_e} + \boldsymbol{F}_{V_H},$$

Nonlinear term:

$$v_{e_i} = \sum_{j=1}^{n_{e_i}} w_{e_{i,j}} u_{e_{i,j}}$$

$$[\eta\,\boldsymbol{k}\times\boldsymbol{V}_H]_{e_i} = \sum_{j=1}^{n_{e_i}} \frac{1}{2}(\eta_{e_i} + \eta_{e_{i,j}})\, w_{e_{i,j}} \rho_{e_{i,j}} u_{e_{i,j}}$$

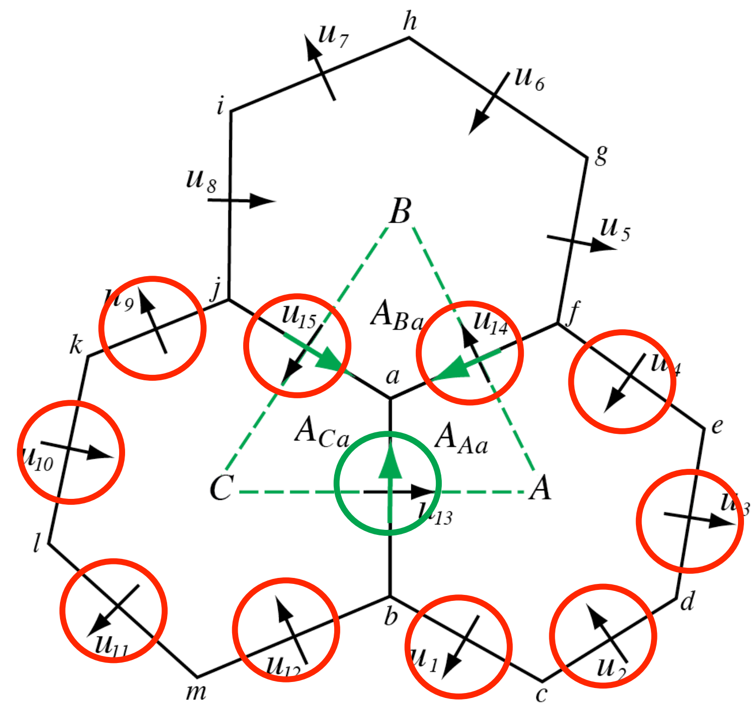

The general tangential velocity reconstruction produces a consistent divergence on the primal and dual grids, and allows for PV, enstrophy and energy* conservation in the nonlinear SW solver.

MPAS-A simulations on Yellowstone

Global, uniform resolution.

6 simulations using average cell-center spacings:

60, 30, 15, 7.5 (2 - with and without convective param) and 3 km.

Cells in a horizontal plane: 163,842 (60 km), 655,362 (30 km), 2,621,442 (15 km), 10,485,762 (7.5 km) and 65,536,002 (3 km).

41 vertical levels, WRF-NRCM physics, prescribed SSTs.

Hindcast periods:
23 October – 2 November 2010
27 August – 1 September 2010, active TC period
15 January – 4 February 2009, MJO event

MPAS Physics:
WSM6 cloud microphysics
Tiedtke convection
Monin-Obukhov surface layer
YSU pbl, Noah land-surface
RRTMG lw and sw.

MPAS
Model for Prediction Across Scales

3 km global MPAS-A simulation 2010-10-23 init

Tropical cyclone Chaba (cat 3)

Observed extratropical cyclone with the lowest recorded surface pressure in North America

Isolated tornadic storms observed in warm sector ahead of the cold front

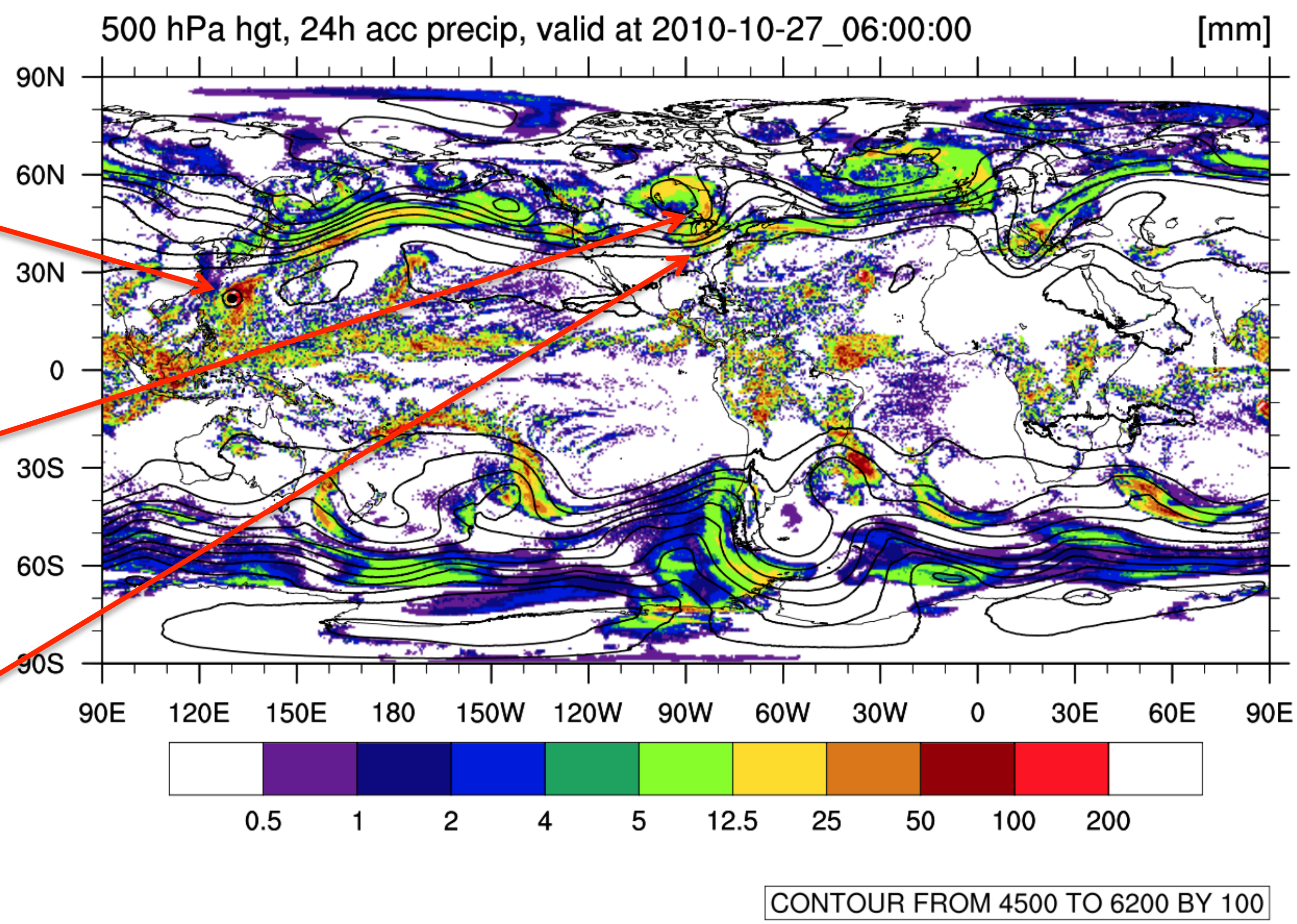

3 km global MPAS-A simulation
2010-10-23 init

MPAS
Model for Prediction Across Scales

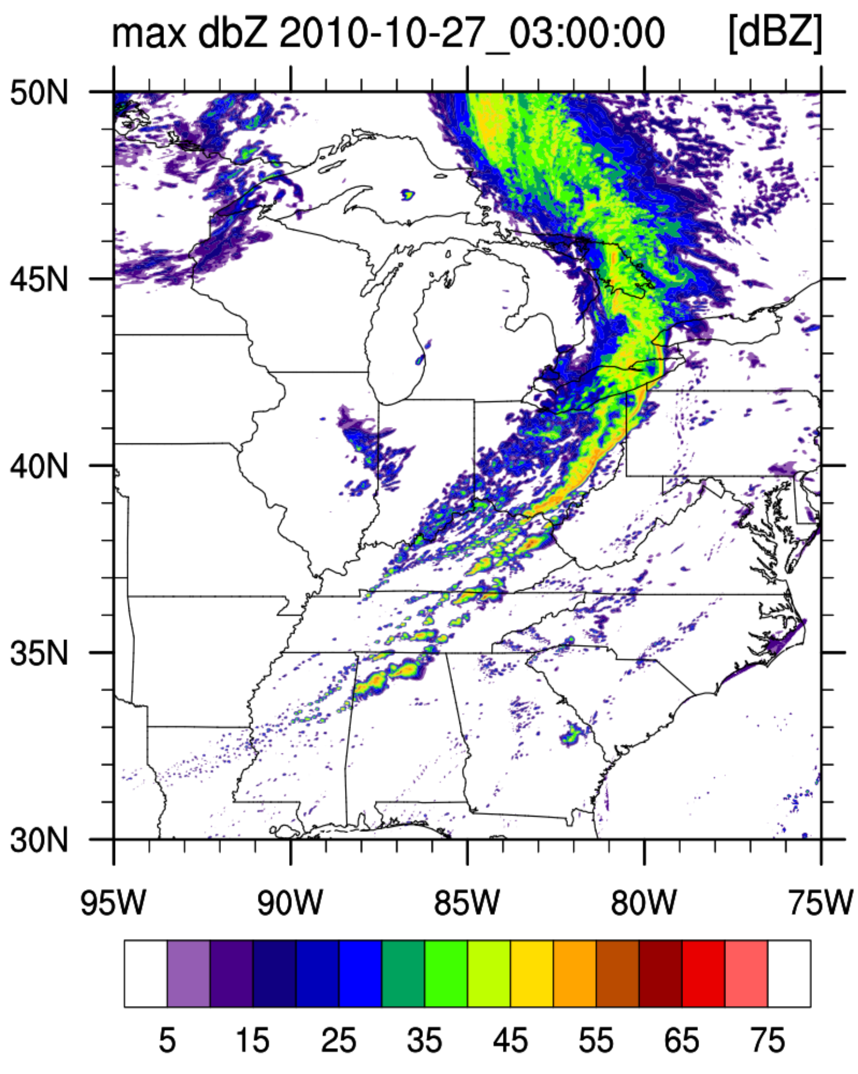

GOES East, 2010-10-27 0 UTC
IR - vapor channel

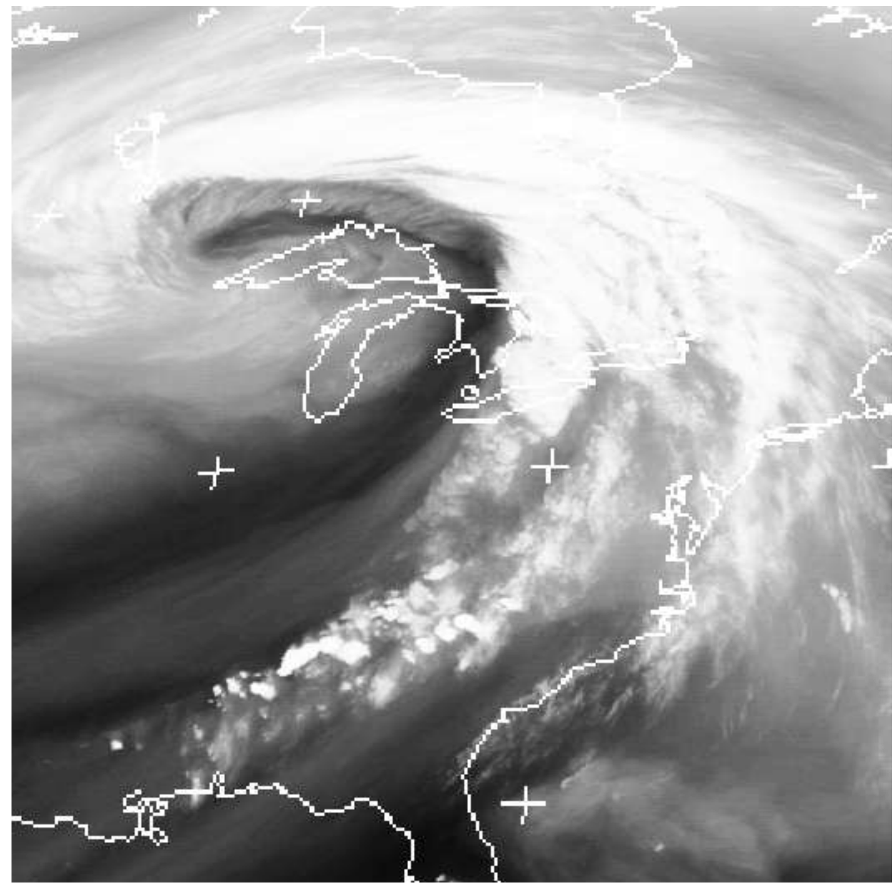

MPAS
Model for Prediction Across Scales

3 km global MPAS-A simulation 2010-10-23 init

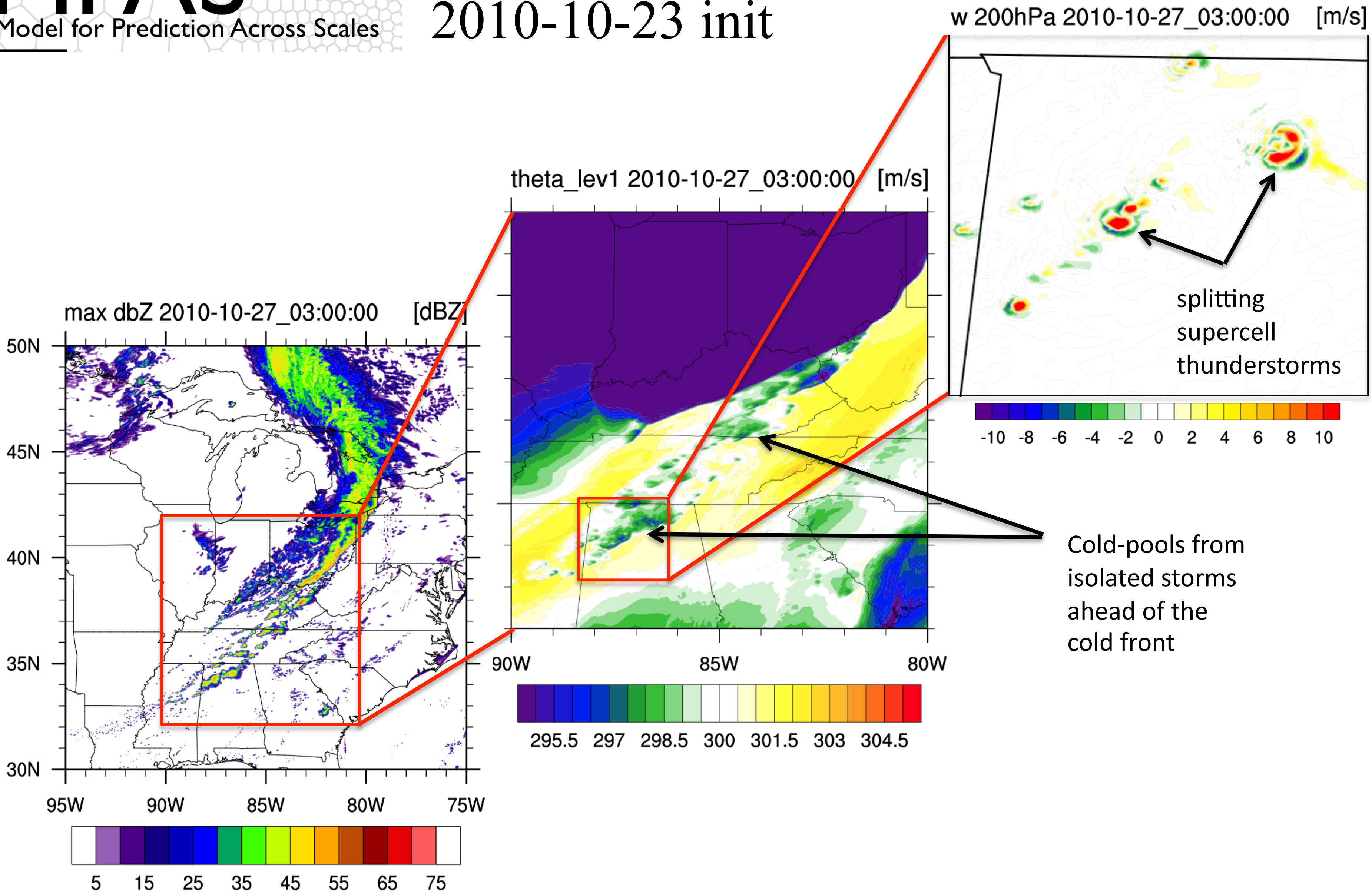

3 km global MPAS-A simulation
2010-10-23 init

Typhoon Chaba

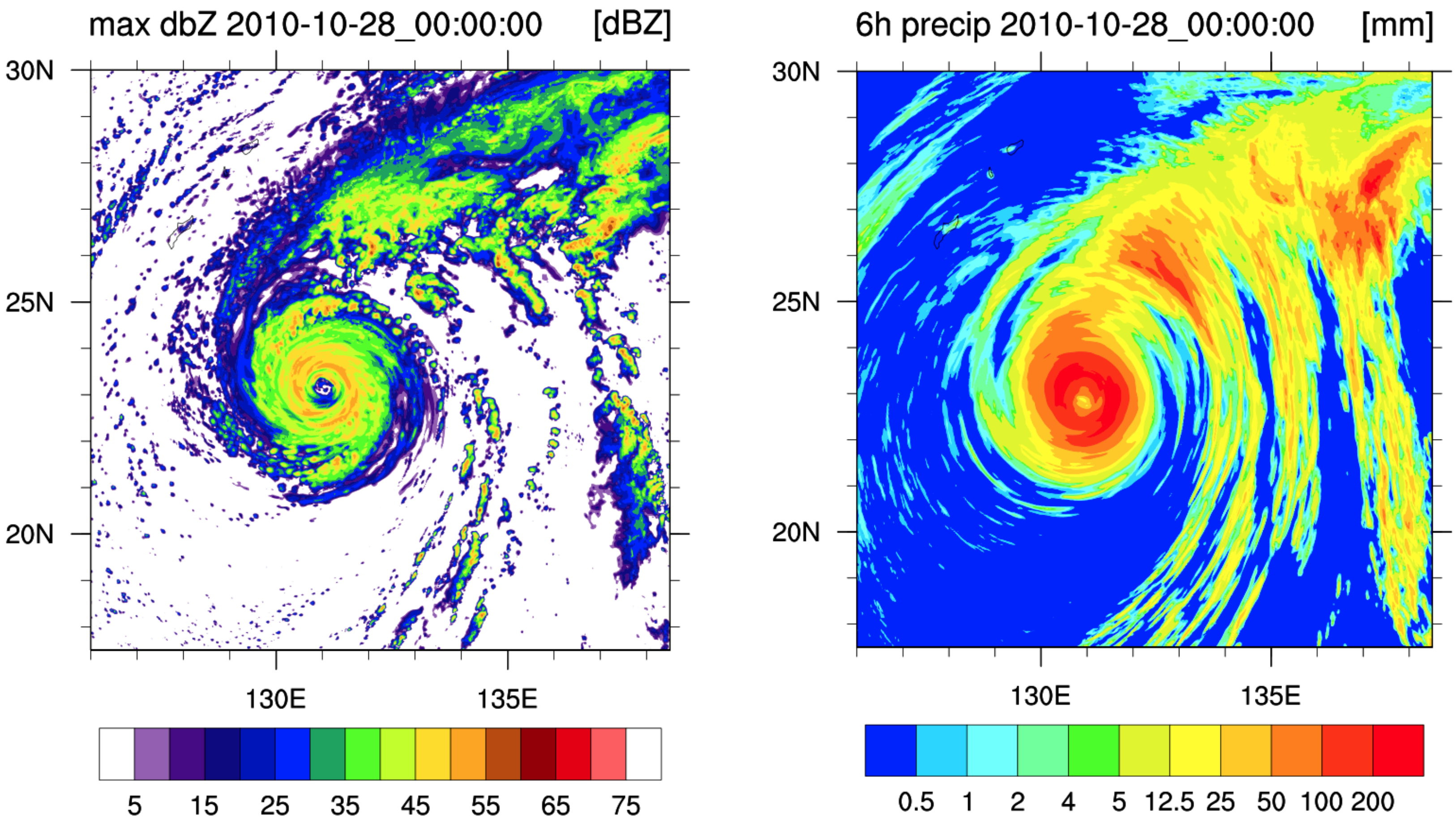

3 km global MPAS simulation 2010-10-23 init

Tropical cyclone Chaba (cat 3)

Tropical cyclone Richard (cat 2)

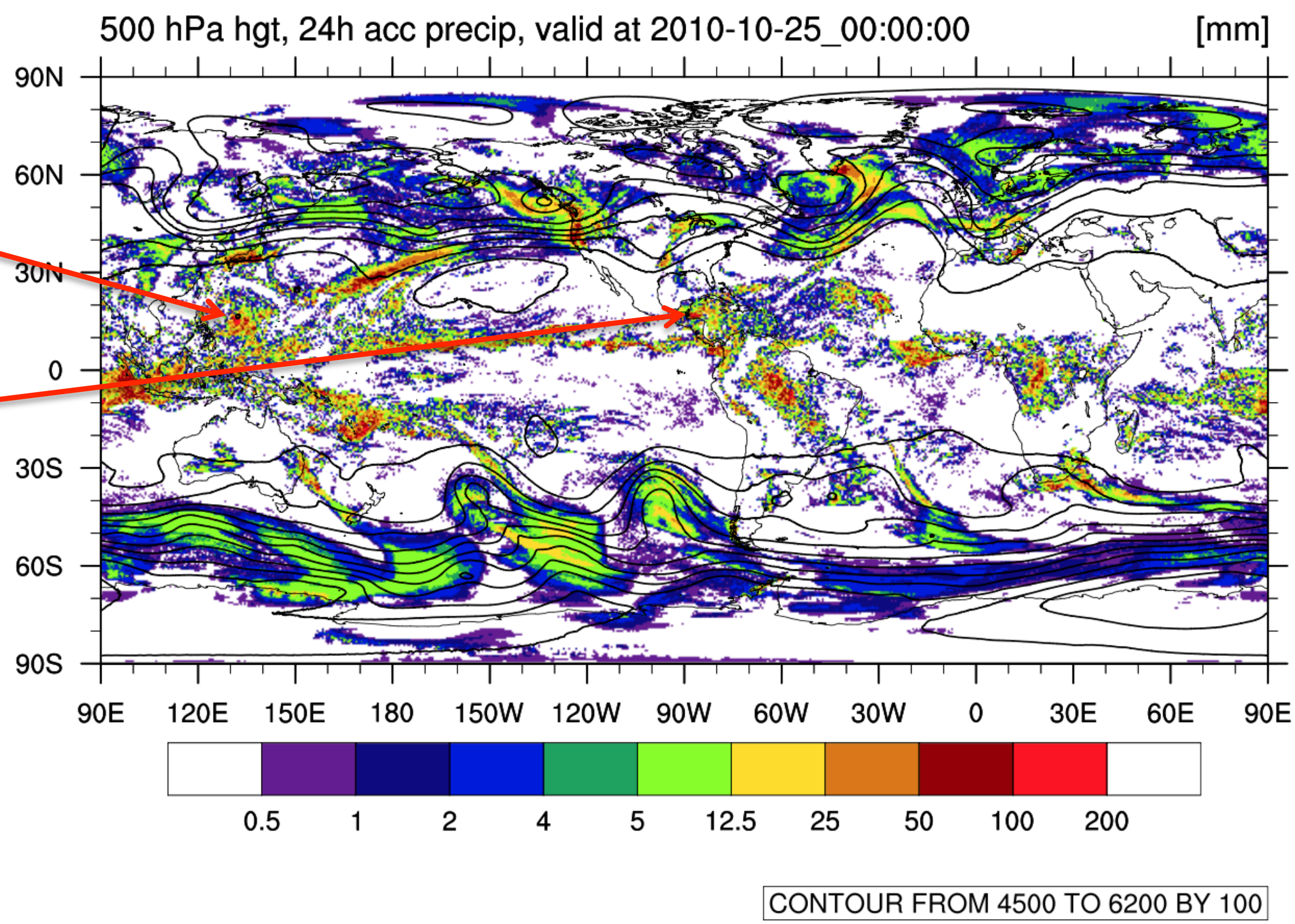

MPAS
Model for Prediction Across Scales

3 km global MPAS simulation 2010-10-23 init

Hurricane Richard

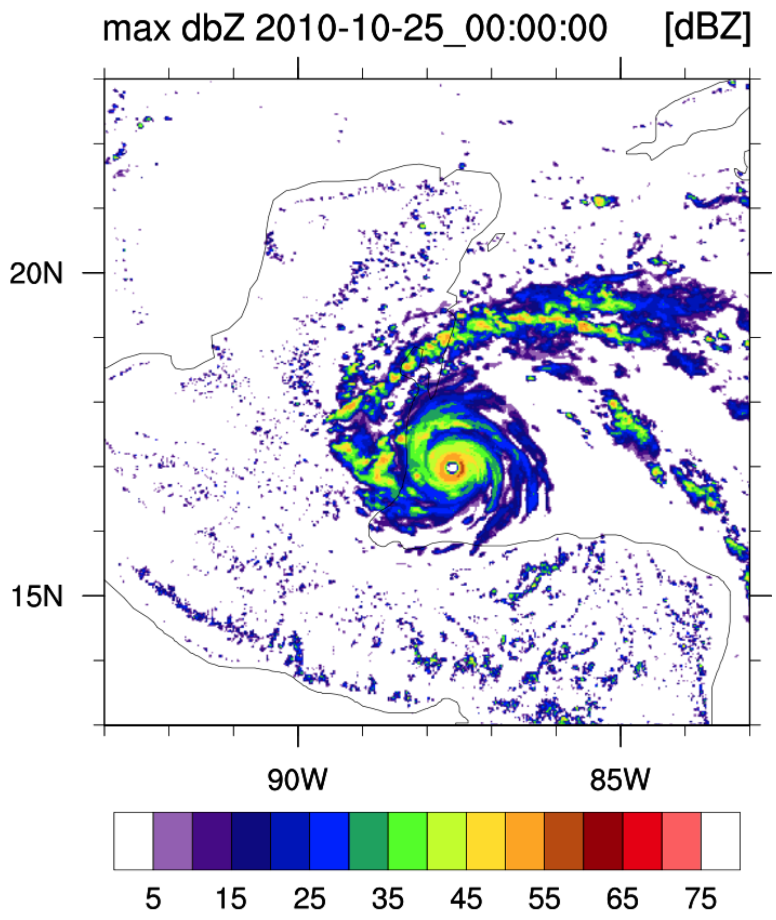

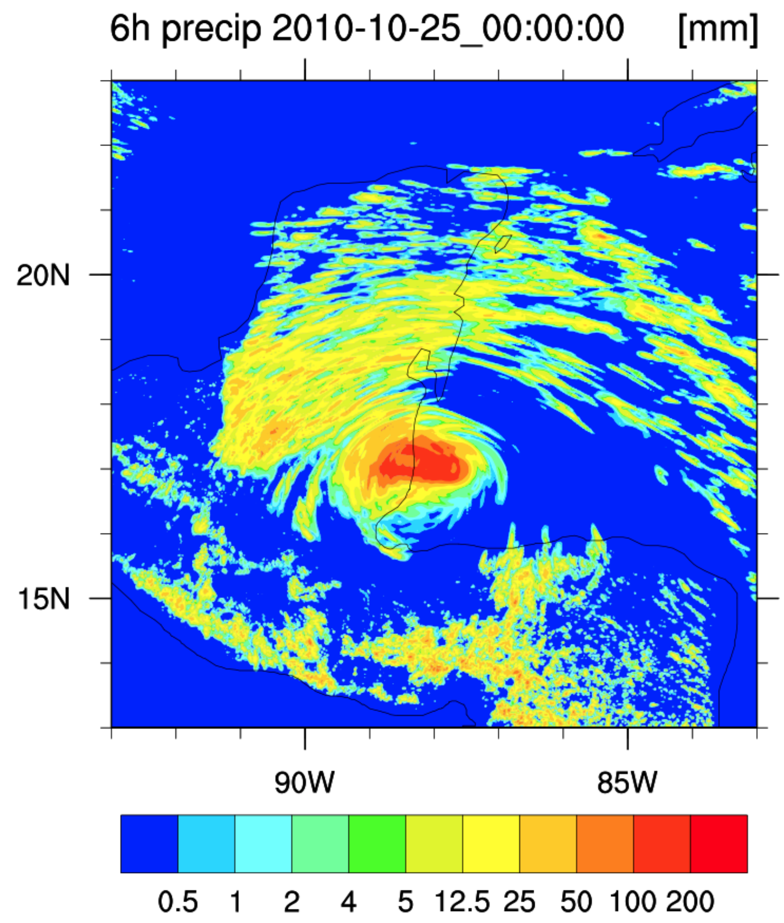

MPAS global simulations, TC Richard

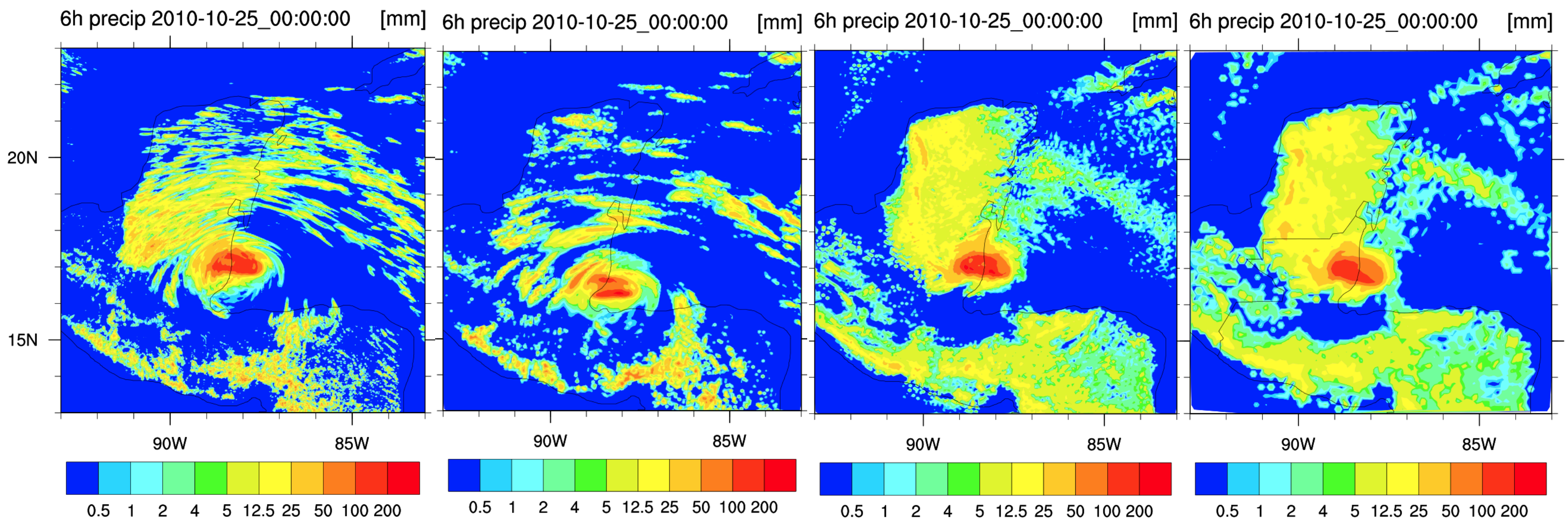

3 km

7.5 km
no convective
parameterization

7.5 km
KF convective
parameterization

15 km
KF convective
parameterization

MPAS
Model for Prediction Across Scales

Precipitation statistics 2010-10-23 init

Averaged precipitation rates are computed for each 6-hour period in the forecast (0-6, 6-12, etc) and plotted at the midpoint of the period.

5-day time average over forecast days 2 - 6

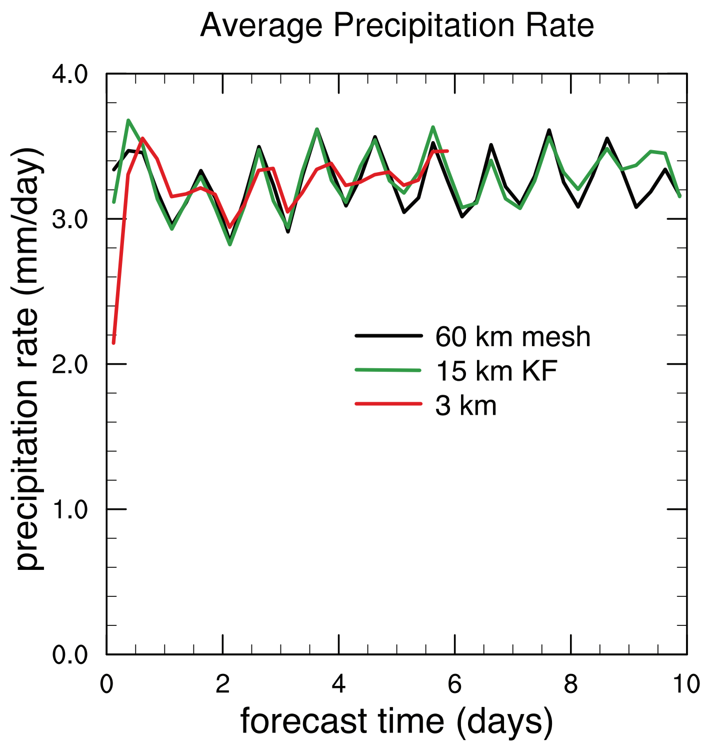

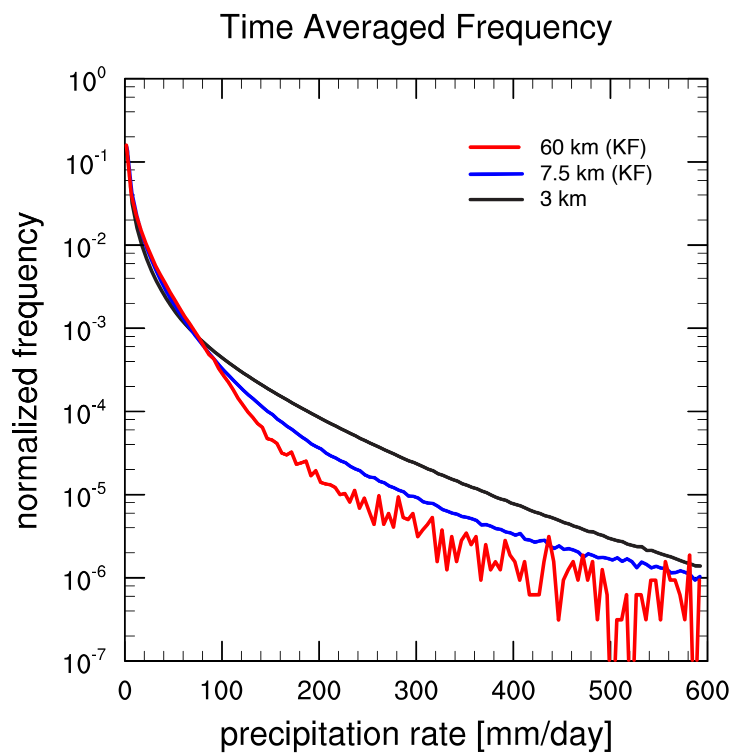

Precipitation statistics 2009-01-15 init

Africa: 10E - 40E, 10N - 20S
3 day average, 17-20 January,
7.5 and 15 km global meshes

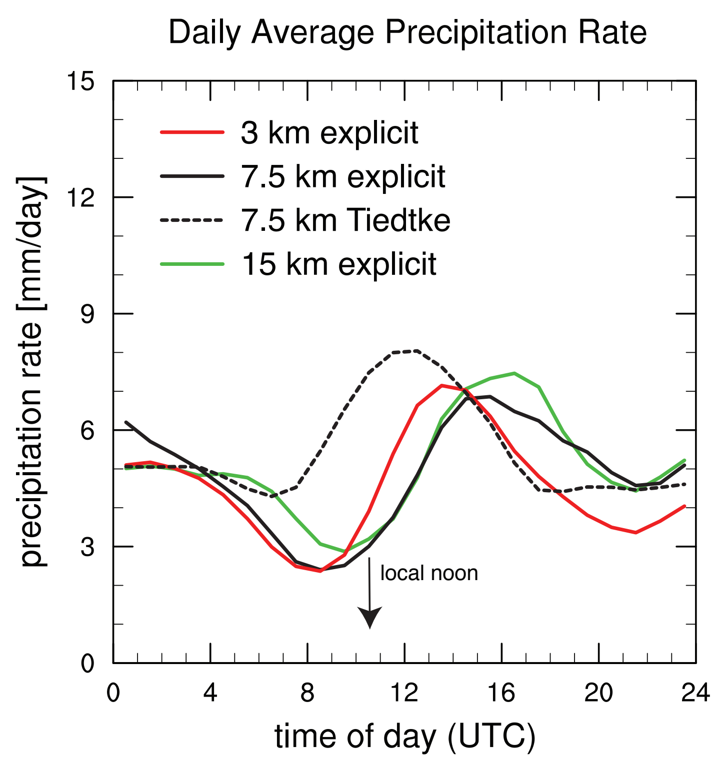

3 km global MPAS simulation

2009-01-15 init, 20 day simulation

KE spectra averaged over 2009-01-20 to 01-30

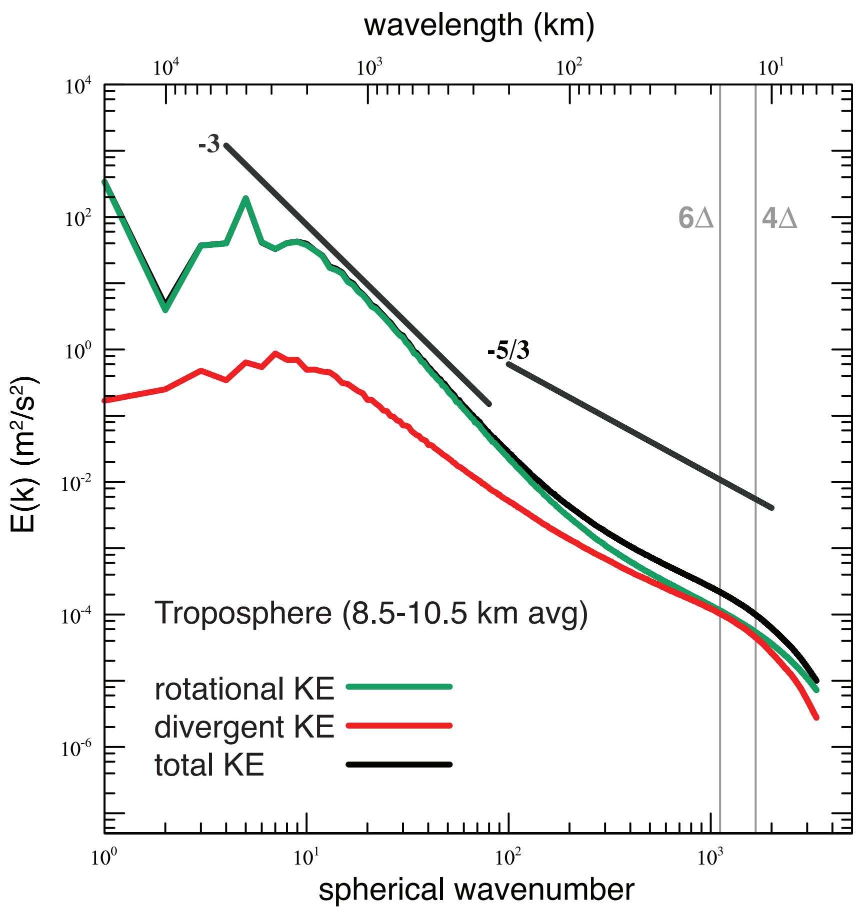

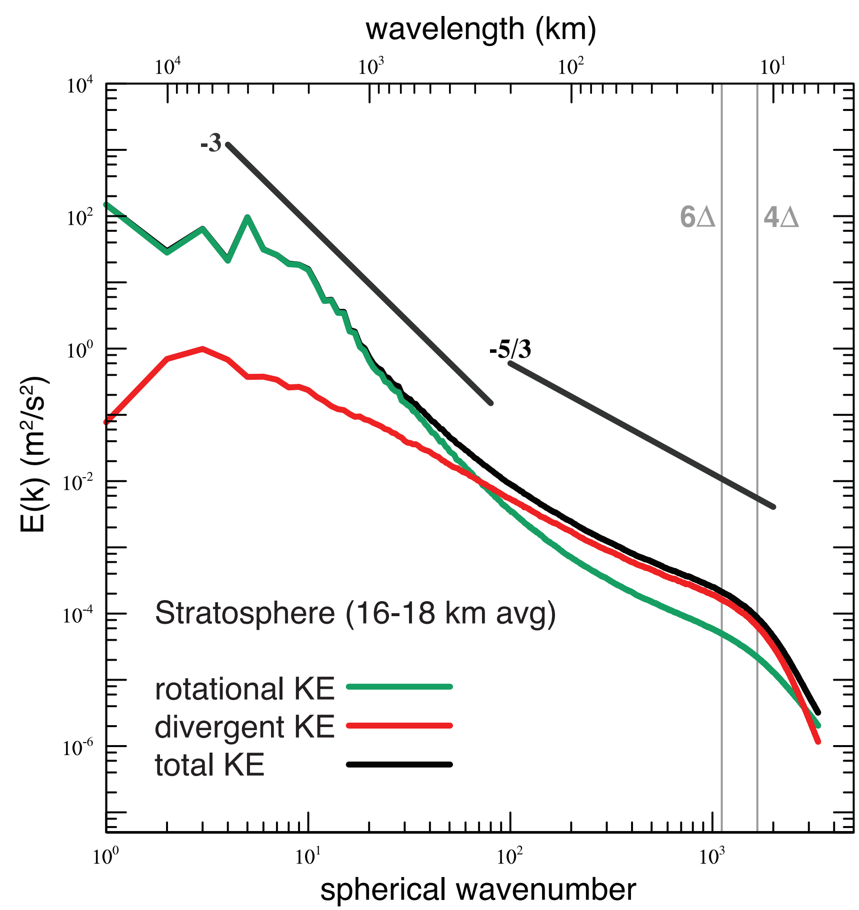

15 km MPAS Coordinate Smoothing
Tibetan Plateau, 28º N

Init. 10-28-10-00Z, Valid 10-29-10-06Z

Terrain height

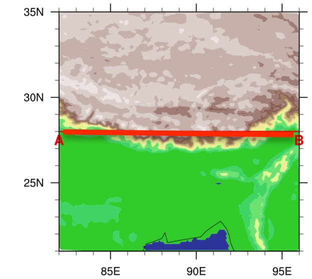

Smoothed hybrid terrain-following (STF) coordinate

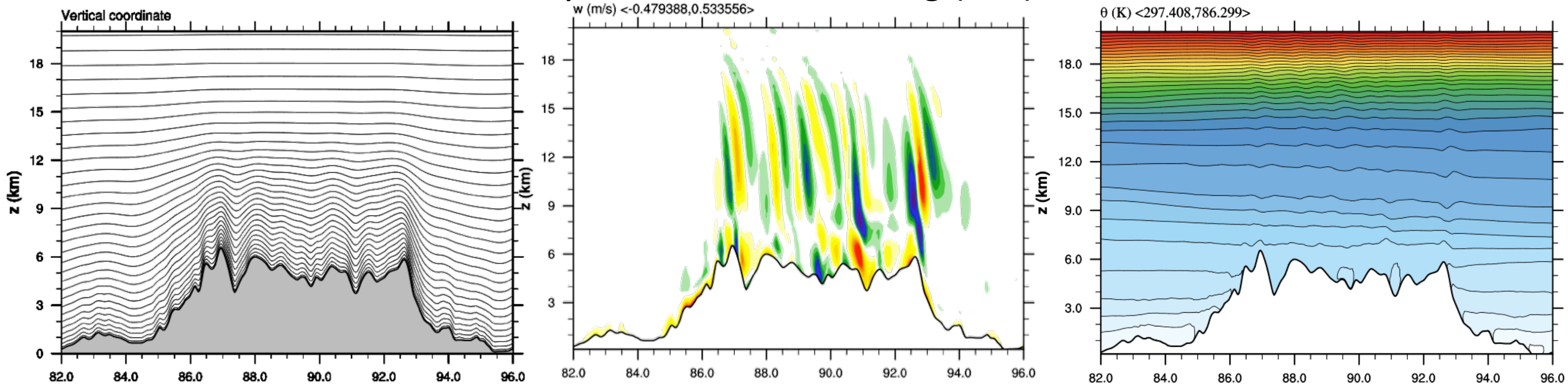

Basic terrain-following (BTF) coordinate

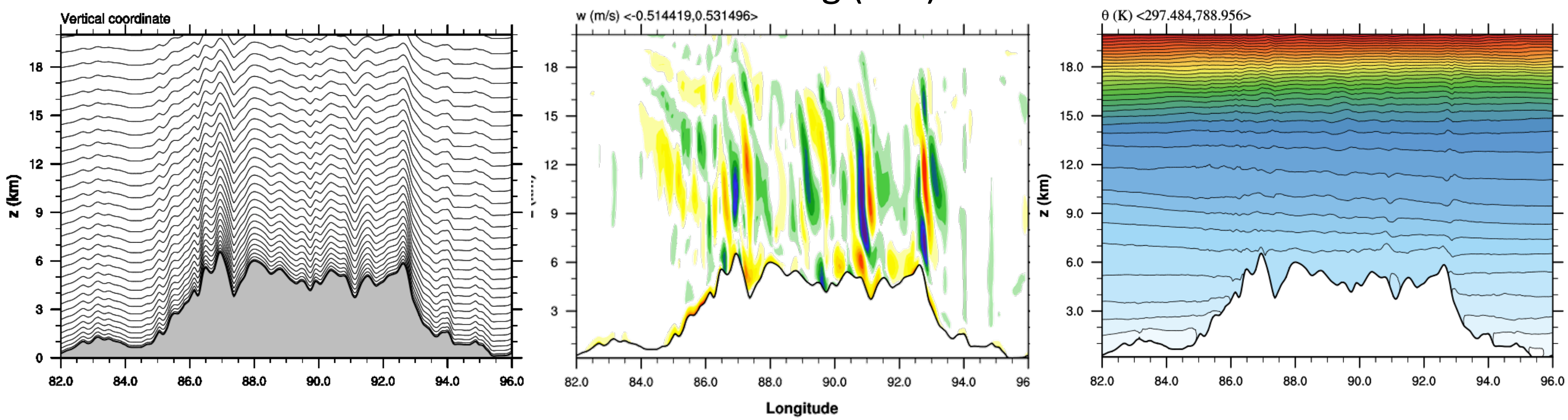

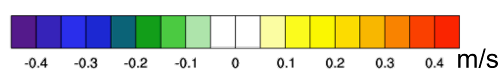

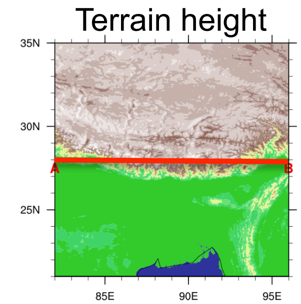

MPAS 15 January 2009 init.
Tibetan Plateau at 28^{o} N

Valid 01-16-2009 00Z

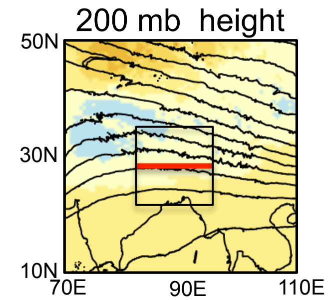

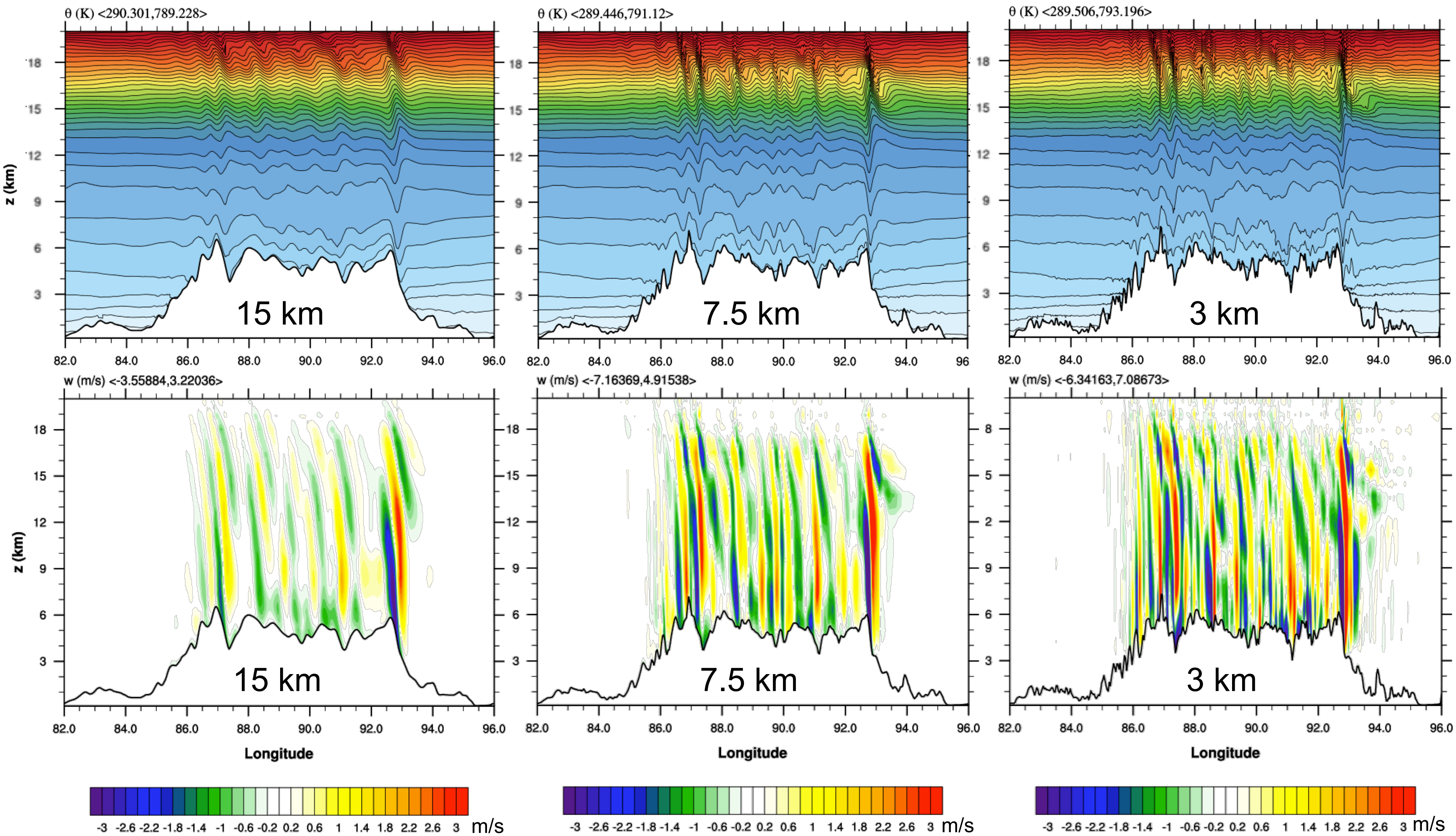

MPAS-Atmosphere 2013 Tropical Cyclone Forecast Experiment

Two different meshes are being used:
(1) A quasi-uniform 15 km (mean cell spacing) mesh.
(2) A variable-resolution mesh (60 - 15 km cell spacing) with the high-resolution region centered over the Atlantic.

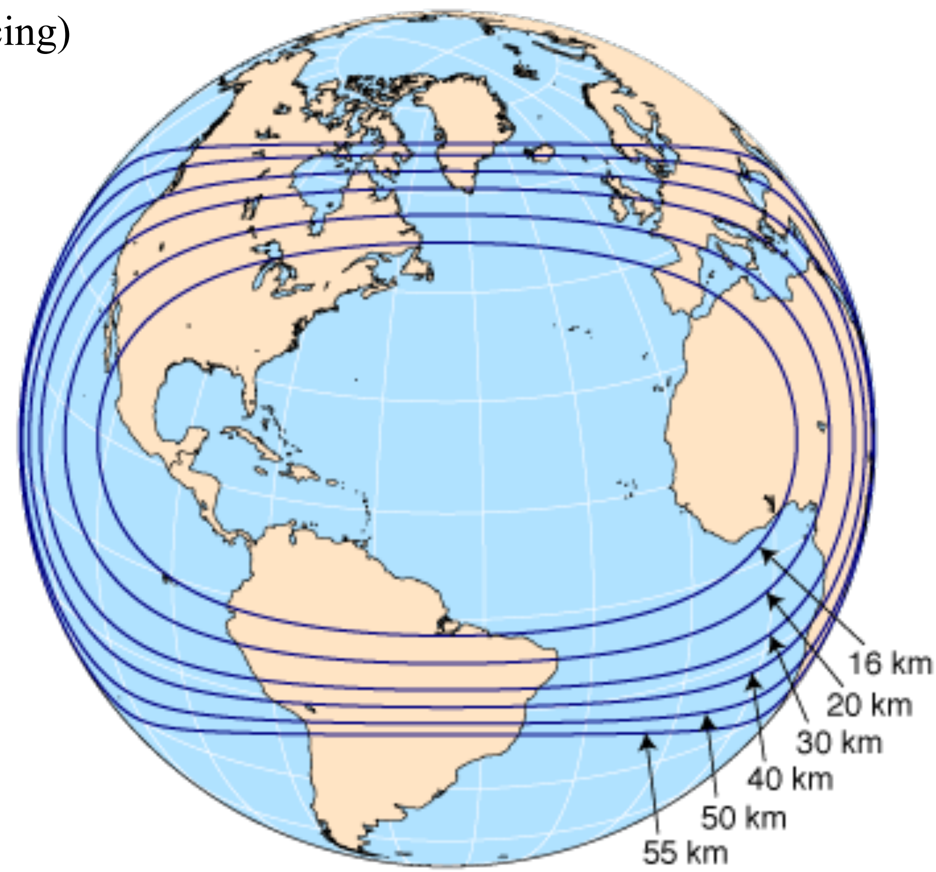

The 15 km mesh uses 2,621,442 cells to tile the sphere (i.e. cells on a horizontal plane), and the variable-resolution mesh uses 535,554 cells to tile the sphere. 41 vertical levels are used. The timestep is 50 s.

<u>Physics</u>

Surface Layer: (Monin Obukhov):
module_sf_sfclay.F as in WRF 3.5.
PBL: YSU as in WRF 3.4.1.
Land Surface Model (NOAH 4-layers):
as in WRF 3.3.1.
Gravity Wave Drag: none
Convection: Tiedtke: as in WRFV3.3.1.
Microphysics: WSM6: as in WRF 3.5
Radiation: RRTMG sw as in WRF 3.4.1; RRTMG lw as in WRF 3.4.1

Variable Resolution Mesh Tests

Δt is constant on the variable-resolution mesh.

Smagorinsky: $K_h = c_s^2 l^2 |Def|$

l^2 scales with Δx^2

Viscosity and hyper-viscosity formulations:

$K_2 \nabla_\zeta^2 \phi$ K_2 scales with Δx^2

$K_4 \nabla_\zeta^2 \left(\nabla_\zeta^2 \phi \right)$ K_4 scales with Δx^4

Locally 2Δ waves are damped at same rate.

MPAS-Atmosphere 2013 Tropical Cyclone Forecast Experiment

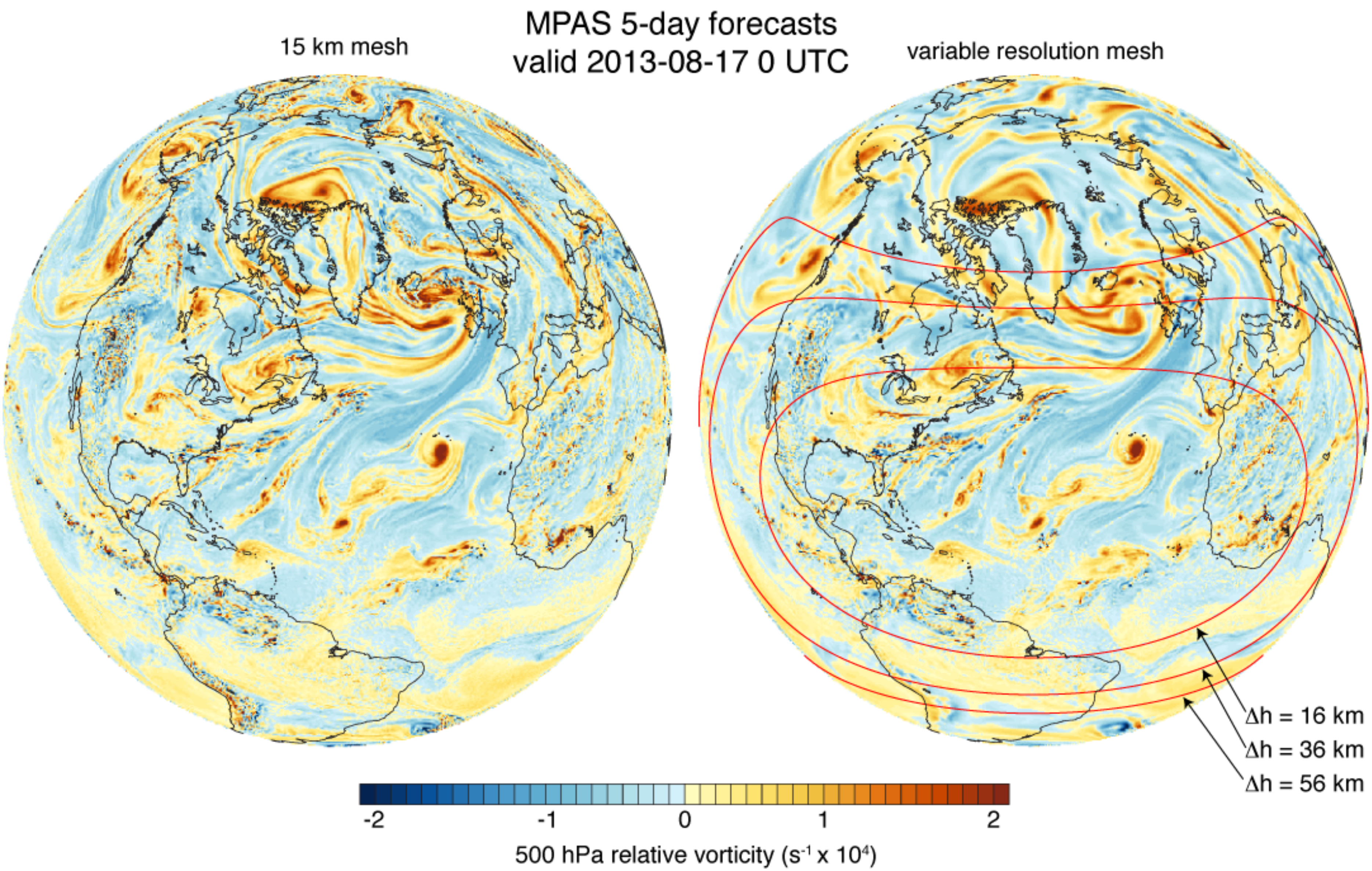

MPAS-Atmosphere 2013 Tropical Cyclone Forecast Experiment

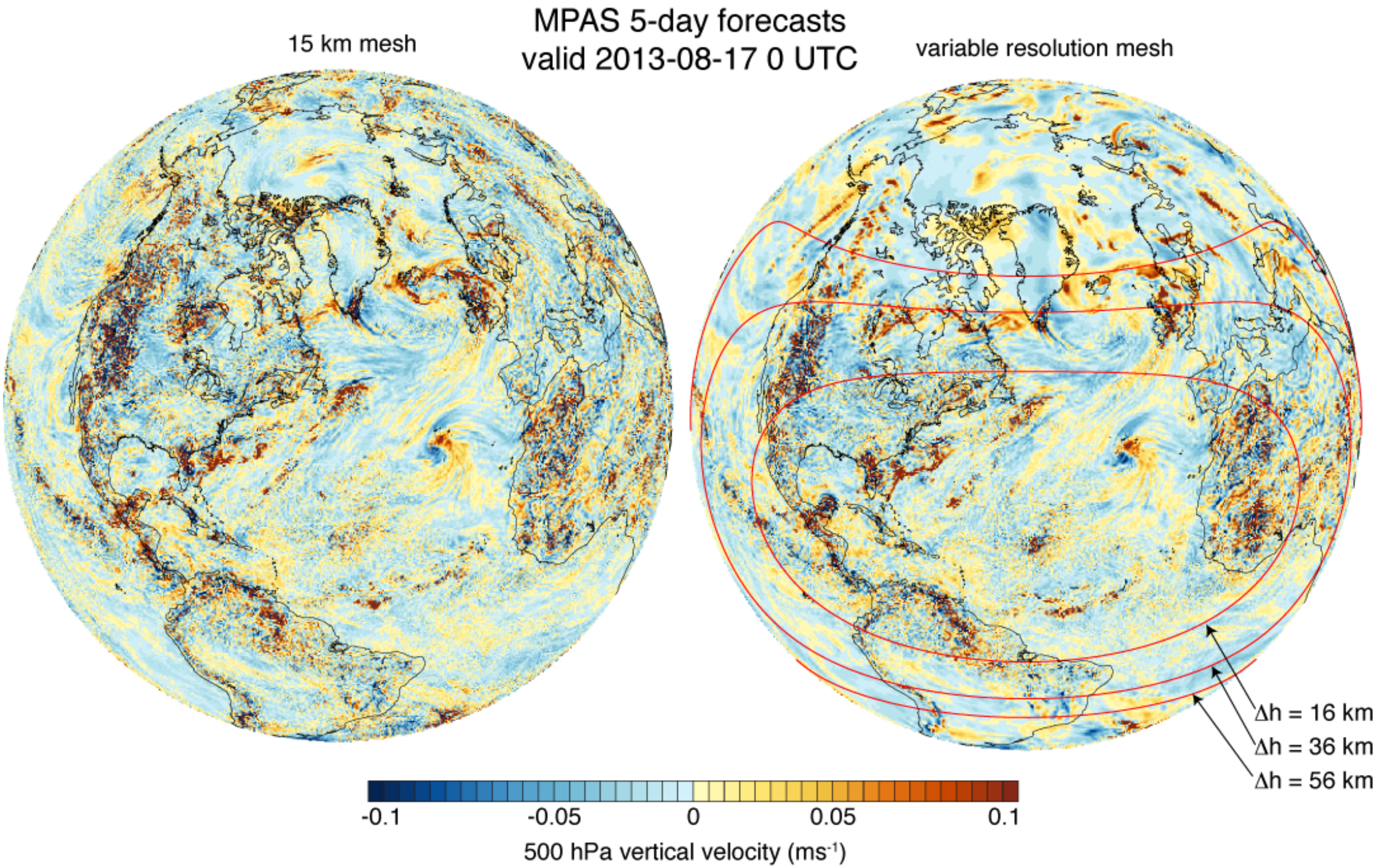

MPAS-Atmosphere 2013 Tropical Cyclone Forecast Experiment

500 hPa Relative Vorticity
2-day forecast valid 2013-08-14 0 UTC

Variable-resolution mesh (dx = 16,36,56 km)

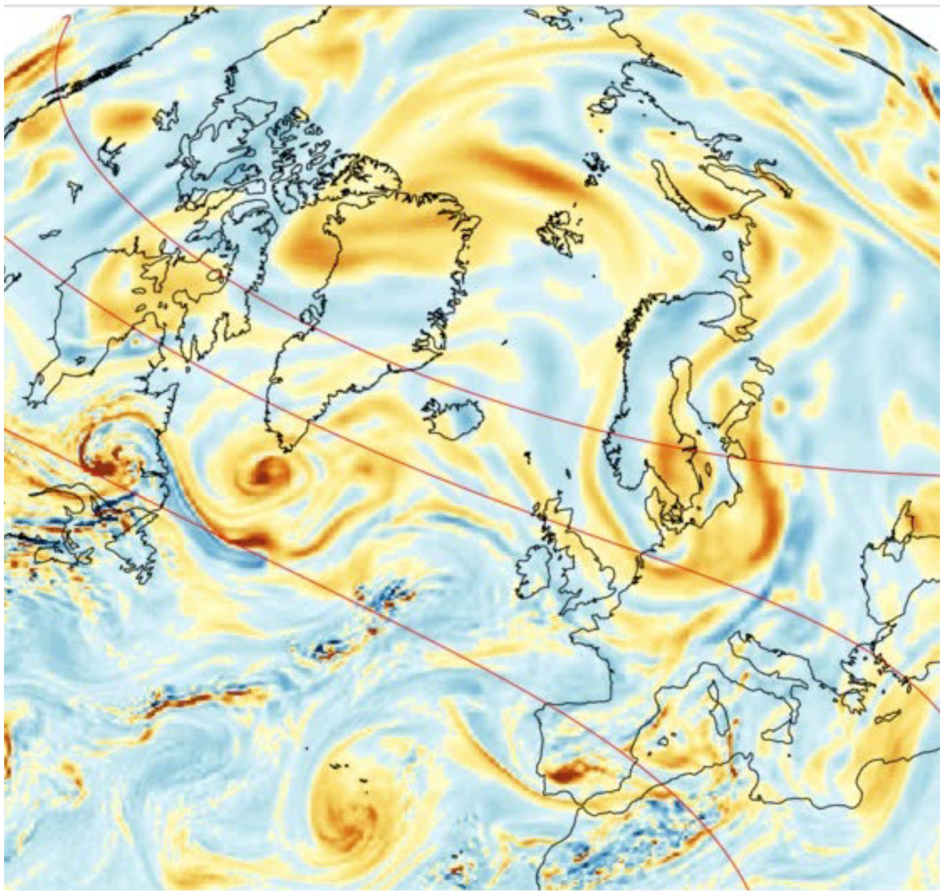

Uniform resolution mesh, dx = 15 km

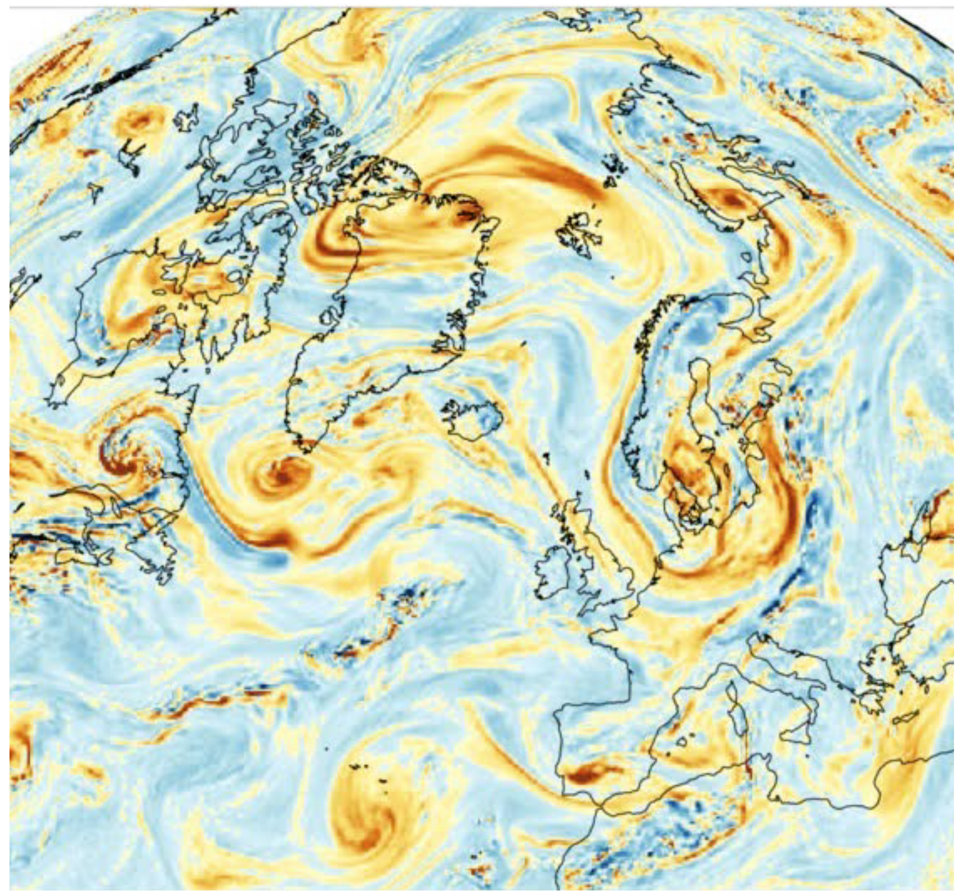

500 hPa relative vorticity, 2013-08-12_00:00:00

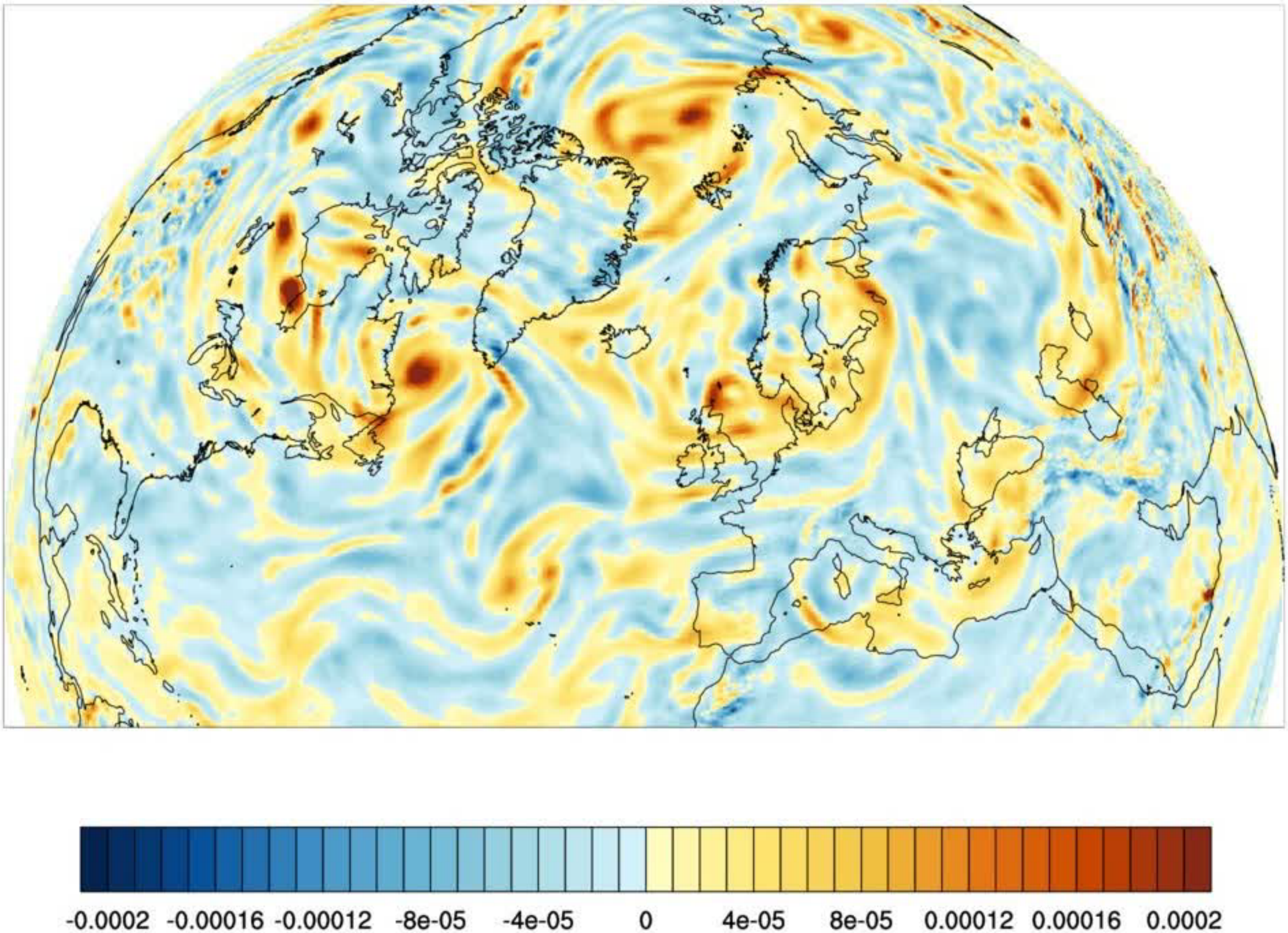

500 hPa relative vorticity, 2013-08-12_00:00:00

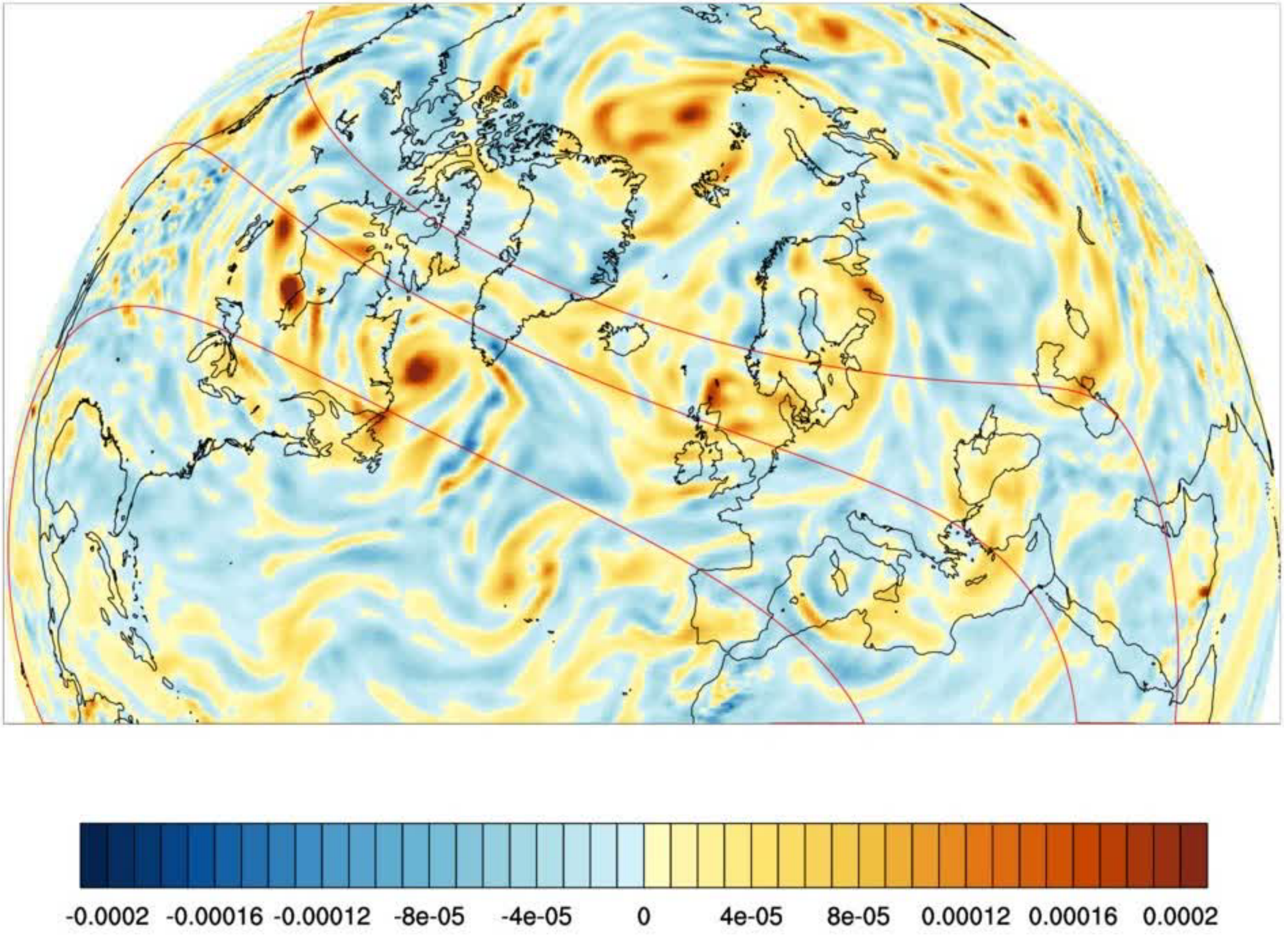

Summary

- Nonhydrostatic atmospheric solvers using C-grid centroidal Voronoi meshes and FV formulations are viable for NWP and climate applications.
- MPAS-Atmosphere (nonhydrostatic) is being tested for full-physics NWP and climate applications. MPAS-Ocean (hydrostatic) is also being tested.
- Variable-resolution results of the MPAS solvers are promising.
- Initial MPI implementations of MPAS-O/A are showing efficiencies and scalings comparable to other models (WRF). Much optimization remains.
- MPAS-A: Our use of variable-resolution meshes is leading us to consider scale-awareness issues in our physics.

Further information and to access MPAS Version 1:
http://mpas-dev.github.io/

MPAS global TC forecast experiment:
http://wrf-model.org/plots/realtime_mpas.php

MPAS Model for Prediction Across Scales   Los Alamos NATIONAL LABORATORY EST. 1943   U.S. DEPARTMENT OF ENERGY Office of Science   NSF   NESL